

A Statistical Framework to Identify Kinematically Outlying LMC Globular Clusters and Implications for the LMC’s Dark Matter Profile

TAMOJEET ROYCHOWDHURY ^{1,2} NAVDHA ^{3,4} HIMANSH RATHORE ⁵ AND KNUT A.G. OLSEN ⁶

¹*Department of Astronomy, University of California Berkeley, Berkeley, CA 94704, USA*

²*Department of Electrical Engineering, Indian Institute of Technology Bombay, Mumbai, 400076, India*

³*Perimeter Institute for Theoretical Physics, 31 Caroline Street North, Waterloo, ON, N2L 2Y5, Canada*

⁴*Department of Physics, Indian Institute of Technology Bombay, Mumbai, 400076, India*

⁵*Department of Astronomy and Steward Observatory, University of Arizona, 933 North Cherry Avenue, Tucson, AZ 85721, USA*

⁶*NSF National Optical-Infrared Astronomy Research Laboratory, 950 North Cherry Avenue, Tucson, AZ 85719, USA*

ABSTRACT

The LMC’s Globular Clusters (GCs) bring a novel opportunity to understand the LMC’s assembly history and dark matter (DM) properties, provided the kinematically outlying GCs can be reliably identified. However, traditional diagnostics like the Energy – Angular Momentum space fail because of large uncertainties on the GC velocities. In this work, we develop a new, robust statistical framework for identifying kinematically outlying LMC GCs, by using their Gaia-DR3 Proper Motions (PMs) combined with previous Line-of-Sight (LoS) velocity measurements. We use the difference between a GC’s velocity vector and the average velocity vector of the surrounding red clump stars as a metric for quantifying a GC’s kinematic peculiarity. We account for both the velocity measurement uncertainties and the LMC’s intrinsic velocity dispersion. We find 5 LMC GCs to be kinematically outlying based on PM differences alone, and additional 6 GCs if LoS velocity information is also used. Majority of the GCs with outlying PMs are clustered at a distance of 3 – 4 kpc from the LMC center. The inclusion of outlying LMC GCs introduces a bias of upto 30% in the LMC’s enclosed mass estimates derived using GCs as dynamical tracers; caution must be exercised in choosing the GC sample for precisely determining the LMC’s DM content. We discuss the possibility that the kinematically outlying LMC GCs may have been accreted from external galaxies, and motivate future spectroscopic follow-up of the GC population to better understand the assembly history of massive satellite galaxies of Milky Way like hosts.

Keywords: LMC (903); Globular Clusters (656); Galaxy kinematics (602); Astronomical methods (1043); Dwarf galaxies (416)

1. INTRODUCTION

The LMC is the most massive ($\sim 10^{11} M_{\odot}$, e.g. Watkins et al. 2024) satellite galaxy of the Milky Way (MW), and is the nearest (≈ 50 kpc away, Pietrzyński et al. 2013) galaxy with a well-formed disk (e.g. van der Marel et al. 2002; Choi et al. 2022; Dhanush et al. 2024). Precision astrometry from Gaia (Gaia Collaboration et al. 2021) and Hubble Space Telescope (HST) (Kallivayalil et al. 2013) have enabled the use of stellar kinematics and cluster kinematics as a valuable tracer of

assembly histories of satellite galaxies like the LMC. Further, these rich kinematic data make the LMC a new laboratory for dark matter (DM) physics (e.g. Besla et al. 2019; Foote et al. 2023; Reynoso-Cordova et al. 2024; DeBrae et al. 2025; Rathore et al. 2025a). Three dimensional velocity vectors of the LMC’s Globular Clusters (GCs)¹ are finally available (Bennet et al. 2022, hereafter B22), which allows studying the LMC’s assembly

¹ While the term “globular cluster” is often used to refer only to those massive, spherical star clusters that are old and metal-poor, in this paper we adopt the definition from the [Unified Astronomy Thesaurus](#), which allows the inclusion of clusters of any age and metallicity.

history and DM properties with the GC population. A detailed identification of kinematically typical and atypical LMC GCs is necessary for effectively utilizing the GC kinematics as a tracer of the LMC’s assembly history and DM content. In this work, we build a statistical framework for identifying kinematically outlying LMC GCs.

The LMC has an abundant GC population, with ≈ 50 GCs identified till date, including 15 old (≥ 10 Gyr in age) clusters (Sarajedini 2024) and several young massive clusters (Johnson et al. 2001; Perina et al. 2010; Ahumada et al. 2019). The LMC likely had a rich assembly history prior to its recent (1–2 Gyr, Besla et al. 2007) infall into the MW halo (e.g. D’Onghia & Lake 2008; Sales et al. 2011; Jethwa et al. 2016; Dooley et al. 2017; Jahn et al. 2022). Further, in addition to the SMC, at least 9 dwarf galaxies in the MW’s neighborhood are either LMC satellites or have interacted significantly with the LMC over the last ~ 1 Gyr (e.g. Patel et al. 2020; Erkal & Belokurov 2020; Pace et al. 2022; Makarov et al. 2023). Hence, a subset of the LMC GCs are possibly accreted from other galaxies. The kinematics of the GCs potentially encode whether they were born in-situ in the LMC, or brought-in from other galaxies.

Kinematics of the MW GC’s have transformed our understanding of the MW’s accretion history (e.g. Carraro et al. 1998; West et al. 2004; Mackey & Gilmore 2004; Myeong et al. 2018; Helmi et al. 2018; Massari et al. 2019; Kruijssen et al. 2019; Pagnini et al. 2023) and DM profile (Battaglia et al. 2005; Binney & Wong 2017; Posti & Helmi 2019; Correa Magnus & Vasiliev 2022). At least 1/4 of the MW GCs are accreted from other galaxies as opposed to forming in-situ (e.g. Forbes & Bridges 2010). The inference of the MW’s merger history from its GCs relies on identifying kinematically outlying GCs that are likely brought in from other galaxies. Kinematically outlying MW GCs are usually identified from the Energy (E) - Specific Angular Momentum (L_z) distribution of the GC population (e.g. Helmi et al. 2018; Belokurov & Kravtsov 2024; Cowley & Stencel 2024). Motivated by this approach, in Figure 1, we place the LMC GC population in the LMC’s E - L_z space. The large measurement errors on the LMC GC kinematics make it very challenging to ascertain kinematically outlying GCs with traditional diagnostics like the E - L_z space. A new methodology is needed to identify kinematically outlying LMC GCs.

Unlike the MW, most of the LMC GCs share the same rotation pattern as the LMC’s disk and are consistent with being in the disk plane (Schommer et al. 1992; Mackey & Gilmore 2003; McLaughlin & van der Marel

2005; Bennet et al. 2022). Hence, comparing the GC velocity vectors to the velocity vectors of stars surrounding the GC in the LMC disk is a promising approach for identifying kinematically outlying GCs. However, this approach has several challenges that need to be addressed.

The LMC’s disk has a significant velocity dispersion (average $v_{rot}/\sigma = 2.9 \pm 0.9$, van der Marel et al. 2002). The intrinsic velocity dispersion must be accounted for when comparing GC kinematics with the kinematics of the surrounding stars. Further, spatially correlated systematic errors in the Gaia PM measurements (Gaia Collaboration et al. 2021) and crowding induced incompleteness of star counts (Rathore et al. 2025c) also hinders effective comparison between the GC kinematics and surrounding star kinematics. The age differences between the GCs and the surrounding field stars also needs to be taken into account while interpreting the kinematic differences.

This work has three objectives:

- Build a statistical framework to compare the kinematics of the LMC’s GCs with the surrounding LMC disk stars. In this framework, we shall take into account the LMC’s intrinsic velocity dispersion and the statistical and systematic uncertainties of the Gaia measurements. The impact of diverse GC ages will also be assessed.
- Present a catalog of LMC GCs that are statistically significant kinematic outliers with respect to the surrounding stars in the disk. Such GCs can have an external origin.
- Assess the reliability of using the LMC GC sample as a tracer of the LMC’s DM content.

For building the statistical framework, we follow two different approaches to find GCs with significantly different kinematics from the surrounding disk stars. The first approach (or the “data driven” approach) involves comparing the PM measurements of the GCs with the PMs of the surrounding LMC stars. The second approach (or the “model driven” approach) involves using a LMC kinematic model to derive the expected velocities of the surrounding stars at the location of each GC, and comparing the observed cluster velocities with the model derived velocities.

The data-driven approach allows us to directly take into account the intrinsic velocity dispersion of the LMC’s disk while comparing GC kinematics to the surrounding star kinematics. However, statistical and systematic uncertainties in the PM measurements can affect the inferences from the data-driven approach. The

model-driven approach on the other hand allows us to evaluate a GC as a kinematic outlier independent of the limitations of the observational data. However, models of the LMC disk might not fully account for its disequilibrium (e.g. Choi et al. 2022; Dhanush et al. 2024; Rathore et al. 2025a). Thus, using the data-driven approach and the model-driven approach simultaneously can help overcome the individual limitations of each of these approaches and yield a clean sample of outlying LMC GCs.

Our manuscript is structured as follows. Section 2 presents the selection of LMC GCs and the sample of surrounding disk stars around each GC. In section 3, we build a statistical framework for identifying kinematically outlying GCs. Based on our statistical framework, we present a catalog of kinematically outlying GCs in section 4. In section 5, we place our results in context with previous works, investigate the reliability of the LMC GC sample for measuring the LMC’s DM content, and assess the limitations and caveats of our analysis as well as future prospects. We conclude in section 6.

2. DATA SELECTION

2.1. Selection of LMC Globular Clusters

We utilize the catalog provided by Bennet et al. (2022, hereafter B22) for the properties of the LMC GCs. B22 provide 6-D phase space information - Right Ascension (RA), Declination (DEC), parallax, proper motion (PM) and radial velocity (RV) along with the associated errors for a sample of 30 LMC GCs. The PMs of the GCs have been obtained by combining astrometry from *Gaia* DR3 and the Hubble Space Telescope (HST).

B22 carefully evaluated the membership probability of the candidate stars belonging to a GC using a maximum likelihood estimation algorithm. They define the likelihood with a Gaussian Mixture Model, which is constructed by combining the positions, PMs, parallaxes and the location of the stars in the color-magnitude diagram (CMD). Then, they performed iterative Gaussian profile fitting in parallax and PM space and rejected the outlying stars in each iteration, thereby obtaining a clean sample of stars belonging to a particular GC.

B22 obtained the PMs (and their errors) of the GCs as a whole by applying the *GetGaia* pipeline (del Pino et al. 2021; Martínez-García et al. 2021) on the cleaned sample of member stars. For GCs with archival HST measurements, they used the *GaiaHub* pipeline (del Pino et al. 2022) to perform photometric source detection and cross-matching to *Gaia* sources. The final values of the GC properties used in this work are adopted from Table 2 of B22.

2.2. Selection of the Surrounding Stars

The surrounding stars associated with a particular LMC GC are chosen to be the red clump (RC) stars in the vicinity of that GC from the *Gaia* DR3 catalog (Gaia Collaboration 2016; Lindegren et al. 2021; Gaia Collaboration 2022). The choice of RC stars as tracers of the surrounding population is motivated by several factors:

- They are an old stellar population (age > 1 Gyr, Girardi 2016), and hence are good dynamical tracers of a galaxy disk. Several studies on the structure and kinematics of the LMC disk have used the RC population (e.g. Subramanian & Subramanian 2009; Choi et al. 2018; Choi et al. 2022; Rathore et al. 2025c).
- They are similar in age to the dominant population of stars that constitute the GCs (ages between 2 - 12 Gyr, He et al. 2022). However, while the RC populations consist of a range of ages, any one GC typically consists of stars having a narrow distribution of ages. We will assess the effect of age on the GC kinematics later in the manuscript.
- They occupy a well-defined region in the CMD (Castellani et al. 2000), which makes them easy to select with *Gaia* photometry.
- Kinematic models of the LMC based on red clump stars have already been developed Choi et al. (2022, hereafter C22). Hence, utilizing RC stars would ensure consistency when we compare the PMs of the GCs to the model derived velocities at the GC location.

We select RC stars in a surrounding annulus around each GC, using the following algorithm:

- The central sky coordinates (RA & Dec) of each GC are queried from SIMBAD ². If the GC center coordinates are α_0 and δ_0 , and a target surrounding star coordinate (from *Gaia*) are α and δ , then we define:

$$R^2 = (\alpha - \alpha_0)^2 \cos^2 \delta_0 + (\delta - \delta_0)^2 \quad (1)$$

Here, R represents the projected on-sky separation between the GC and a target surrounding star.

- We retrieve all stars residing within an annulus defined by an inner radius R_{in} and an outer radius R_{out} with respect to the GC center (exact

² <https://simbad.cds.unistra.fr/simbad/sim-fid>

choices for R_{in} and R_{out} are explained later in section 2.2.1) satisfying:

1. $1.0 \leq G_{BP} - G_{RP} \leq 1.3$
2. $18.6 \leq \text{phot_g_mean_mag} \leq 19.3$
3. $(\mu_\alpha^* - 1.8593)^2 + (\mu_\delta - 0.3747)^2 \leq 1.5^2$

These selection criteria are motivated from Choi et al. (2022) and Rathore et al. (2025c). Here G_{BP} , G_{RP} and phot_g_mean_mag are the magnitudes in the Gaia blue photometer, red photometer and the G-band. $\mu_\alpha^* = \mu_\alpha \cos \delta$ and μ_δ are the proper motions in RA (declination corrected) and DEC respectively. The criteria (1.) and (2.) select the red clump region in the Gaia CMD. The criteria (3.) ensures that the PMs of the chosen stars are not significantly different from the systemic PM vector of the LMC. The resulting sample of stars were queried from *Gaia* DR3 using the `astroquery.Gaia` Python package ³.

- Finally, to limit contamination from the foreground MW stars, we use LMC membership probabilities as calculated by Jiménez-Arranz et al. (2023, hereafter JA23). JA23 developed a supervised neural network classifier for determining LMC membership probabilities of Gaia sources. We utilized the optimal selection criteria of JA23 to prioritize completeness of LMC stars. We keep only those Gaia sources whose corresponding probability of being an LMC star in JA23 (P_{LMC}) is more than 0.52. Over the entire LMC sample, $\sim 52.3\%$ of the stars get removed by the probability cut. Reassuringly, $\sim 82\%$ of the original sample has either $P_{\text{LMC}} < 0.1$ or > 0.9 , suggesting a clear separation between the LMC stars and the MW foreground contaminants. The probability cut of 0.52 is close to the canonical cutoff of $P > 0.5$ typically used in GC membership probability studies (e.g. Kuzma et al. 2021).

2.2.1. Inner & Outer Radii for Surrounding Star Selection

In this section, we explain in detail our choice for the inner and outer radii of the annuli we defined in section 2.2 for selecting stars surrounding a particular GC. The value of R_{in} is taken to be 0.05 degree for all GCs. Adopting an LMC distance of 50 kpc from Pietrzyński et al. (2013), this angular extent corresponds to a spatial extent of 45 pc. The half-light radii of most globular clusters are about 10 pc or less (van den Bergh 2008)

while r_{90} (radius enclosing 90% luminosity) values are ~ 20 pc (Werchan & Zaritsky 2011). Tidal radii (radius beyond which the galactic gravitational field is stronger than the GC's own field) are 20-50 pc for some representative LMC GCs studied in Piatti & Mackey (2018). Hence, our choice of R_{in} ensures an almost exclusive selection of stars outside of the GC.

We decide R_{out} based on the number of stars present in the annulus. We initially set R_{out} at 0.15° , which yields between 2000 and 3500 surrounding stars for most of the GCs. To ensure uniformity on the number of surrounding stars for each GC, we increase or decrease the value of R_{out} in steps of 0.01° so as to get a count between 2000 and 3500. This range of star counts is necessary for reliable estimation of the mean PM and the PM dispersion of the surrounding star sample, as justified in the paragraphs below.

We use the algorithm developed by Vasiliev (2018, 2019a,b) (hereafter referred to as the V19 code) to estimate the mean PM (with uncertainty) and the PM dispersion of the surrounding star sample. The aforementioned cited works have used this code for analyzing the PMs of the GCs in the Milky Way and the LMC. The V19 code ensures optimal performance with astrometric data at the LMC distance, particularly for crowded fields. We refer the reader to Appendix A of Vasiliev (2019a) for the details of the code, like the treatment of systematic errors in the observed astrometry and the fitting procedure via likelihood maximization to obtain the PM mean and the PM dispersion of a sample of Gaia stars.

Briefly, the $2N$ proper motion components of a set of N stars are assumed to be drawn from a $2N$ -dimensional Gaussian. The N mean values for the μ_α^* and the μ_δ components are assumed to be the same, and denoted as m_α^* and m_δ respectively. The diagonal elements of the covariance matrix used to define the Gaussian have values equal to the quadrature sum of the intrinsic PM dispersion and the measurement uncertainty for the PM component of a star. The off-diagonal element for μ_α^* and μ_δ of the same star is equal to the correlated error in the measurement of μ_α^* and μ_δ . The off-diagonal element corresponding to the PM components of two different stars is taken to be 0. This covariance matrix is then used in a log-likelihood maximization procedure to find the most probable values for the mean PM and the intrinsic PM dispersion. For calculating the PM uncertainties, the Hessian matrix with respect to the model parameters (mean and dispersion of GC PM) is computed.

The V19 code works best when the count of stars in the region of interest is ~ 1000 . The method results in

³ <https://astroquery.readthedocs.io/en/latest/gaia/gaia.html>

progressively higher errors on the returned values (mean PM and dispersion) as the number of stars decreases. For this reason, any GC whose surrounding region has < 200 stars has too high errors ($\geq 0.05 \text{ mas yr}^{-1}$) on the returned PM values, and is consequently rejected from further analysis. The upper error threshold that we adopt ($\geq 0.05 \text{ mas yr}^{-1}$) is defined by observing the typical values of PM differences between the GC and surrounding stars, which are $\sim 0.1 \text{ mas yr}^{-1}$. Hence, if the measurement error in the mean PM is greater than 0.05 mas yr^{-1} , we cannot interpret the kinematic differences between the GC and surrounding PMs. Low counts of surrounding stars primarily happen for the outermost GCs residing in sparser regions of the LMC.

On the other hand, if the star counts in the annuli for the surrounding stars becomes larger than 5000, then the covariance matrix for the two PM components will be of dimensions $10^4 \times 10^4$. Inverting this matrix for the likelihood computation (of the PM distribution) is computationally infeasible. The V19 code performs optimally when the star counts are between 2000 and 3500 (E. Vasiliev *priv. comm.*).

In addition to the above criteria of star counts, we impose a lower limit and an upper limit on what R_{out} can be at 0.1° and 0.2° respectively. The lower limit is chosen so that R_{out} is at least twice R_{in} . The upper limit corresponds to roughly 180 pc at the LMC distance, which is between 3 and 5 times the typical tidal radius of LMC GCs (Piatti & Mackey 2018). Further, beyond an on-sky extent of 0.2° , the spatially-correlated systematic errors between Gaia PMs can no longer be assumed to be constant (P. McMillan *priv. comm.*, see also Gaia Collaboration et al. 2018).

Our surrounding sample of RC stars, therefore is not completely devoid of possible members of the GC itself. However, any contaminants in the sample would only lower the PM difference between the GC and the surrounding stars. GCs having a high difference with our surrounding sample will likely have an even higher difference if a more cleaner sample is selected. Our conclusions will still hold.

2.3. LMC GC's in the Energy - Angular Momentum Space

The specific energy (E) – specific angular momentum (L_z) parameter space has been widely utilized to identify kinematically outlying stellar populations in the Milky Way (e.g. Helmi et al. 2018; Belokurov & Kravtsov 2024; Cowley & Stencel 2024). We apply the same technique on our set of GCs to infer if traditional diagnostics like the $E - L_z$ space provide any insights into significantly outlying LMC GC populations.

For the rest of this paper, we use (r, ϕ, z) to refer to a cylindrical coordinate system centered on the LMC and aligned with its disk plane. The LMC photometric center (RA, DEC = $81.28^\circ, -69.78^\circ$), disk inclination (37.4°) and the coordinate transformation equations for converting the equatorial coordinates to (r, ϕ, z) are taken from van der Marel & Cioni (2001) and van der Marel et al. (2002). A similar reference frame was adopted in the B22 catalog.

We take the values of r , v_ϕ , and the uncertainty in v_ϕ [$\epsilon(v_\phi)$] for the GCs from B22, and compute the specific angular momentum:

$$L_z = r v_\phi \quad (2)$$

and its error:

$$\epsilon(L_z) = r \times \epsilon(v_\phi) \quad (3)$$

The specific kinetic energy of the GCs is computed using the squared sum of residual velocities. The residual velocities are obtained after subtracting the LMC's systemic motion from the total 3-D velocity vectors of the GCs. For the LMC, we adopt $(\mu_\alpha^*, \mu_\delta) = (1.910, 0.229) \text{ mas yr}^{-1}$ (Kallivayalil et al. 2013) and $RV = 262.2 \text{ km s}^{-1}$ (McConnachie 2012). These values for the LMC's systemic motion were also used by B22. The error in kinetic energy is computed as the sum $\sum_i v_i \epsilon_{vi}$, where v_i is the residual velocity component ($\mu_\alpha^*, \mu_\delta, RV$) and ϵ_{vi} is the corresponding uncertainty in that component.

For computing the specific potential energy of the GCs, we model the LMC's dark matter (DM) halo potential as a Hernquist profile (Hernquist 1990), with a total halo mass of $1.8 \times 10^{11} M_\odot$ and a Hernquist scale radius of 23.1 kpc (Patel et al. 2020). The LMC's disk potential is modeled as a Miyamoto-Nagai function (Miyamoto & Nagai 1975), with a total disk mass of $3 \times 10^9 M_\odot$, scale radius of 1.7 kpc and scale height of 0.27 kpc (Patel et al. 2020). Using the r and z values of the GCs from the B22 catalog, we compute the specific potential energy of each GC. With a fixed coordinate system, the uncertainties in the radial distance from LMC centre (r) are small and the total energy uncertainties are dominated by the kinetic energy uncertainties for all GCs.

E is given by the sum of the specific kinetic energy and the specific potential energy. We plot E v/s L_z along with 1σ errorbars in Figure 1. Given the large errorbars on E and L_z , it is challenging to identify GCs that are kinematic outliers from this plot. Clustering of GCs in the $E - L_z$ space is also hard to identify given the large errorbars. We note that two GCs, NGC 2210 and NGC 2159 have $E > 0$ and hence are likely unbound to the LMC, and are obvious kinematic outliers. These two GCs have been considered outliers in previous works as

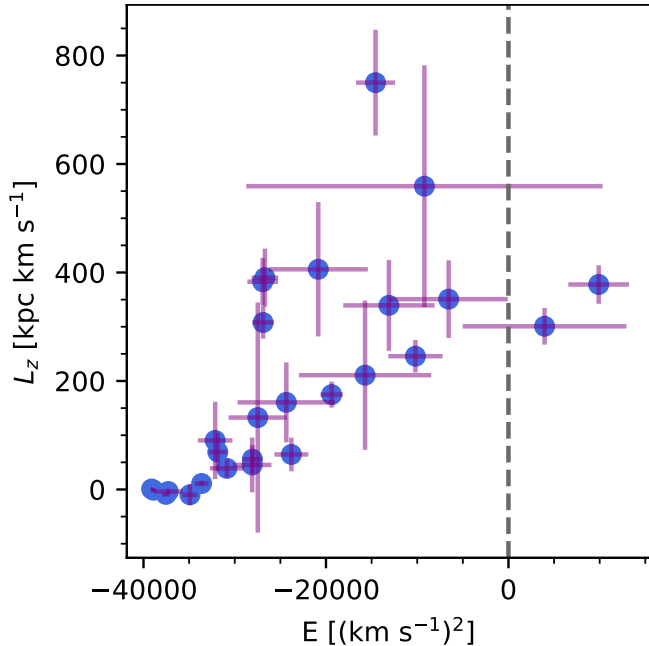


Figure 1. The sample of LMC GCs used in our work is plotted in the specific energy (E , x-axis) v/s specific angular momentum (L_z , y-axis) space, with their 1σ errorbars. The coordinate frame is described at the start of section 2.3. Given the large errorbars on most of the GCs, it is challenging to identify kinematic outliers with traditional diagnostics like the E - L_z space, and a new framework is needed. The grey dashed vertical line marks $E = 0$, and GCs that reside to the right of it (NGC 2210, NGC 2159) are likely unbound to the LMC, making them obvious kinematic outliers.

well, like B22 and Watkins et al. (2024) (we shall see later that our new statistical framework also flags both of these GCs as kinematic outliers).

The inability of the $E - L_z$ space to identify outlying GCs necessitates a framework that directly evaluates the differences between the GC kinematics and the kinematics of the surrounding LMC disk stars. Further, to reliably assess any difference, we need statistically well-defined metrics that account for non-physical (like measurement uncertainties) and physical (non-zero velocity dispersion) agents that can lead to the GC kinematics being different from the surrounding stars.

3. STATISTICAL FRAMEWORK FOR IDENTIFYING OUTLYING LMC GLOBULAR CLUSTERS

We compute the difference between the GC velocities and the velocities of the surrounding stars. To establish statistical significance, we compare the difference with measurement errors as well as the intrinsic velocity dispersion of the surrounding stars. The velocities for the surrounding stars are calculated using two methods. The first method involves directly calculating the

velocities using the Gaia DR3 measurements. The second method involves estimating the velocities using a kinematic model of red clump stars developed by C22.

The GC velocities and their errors are directly adopted from the B22 catalogue. The catalogue reports the mean PM in RA and DEC and their corresponding uncertainties for each GC.

3.1. Surrounding Star Velocities Using Gaia DR3 Dataset

We use the final sample of surrounding stars as selected in section 2.2. We compute the resultant mean PM along RA and DEC, their corresponding uncertainties, and the intrinsic PM dispersion using the V19 code.

3.2. Surrounding Star Velocities Using an LMC Kinematic Model

We use the kinematic model for the LMC's RC disk developed by C22 based on the formalism of van der Marel et al. (2002). We note an important discrepancy in the coordinate system assignment – the adopted LMC center are different in the B22 catalog and the C22 model. B22 uses the LMC photometric center from van der Marel et al. (2002), whereas C22 determine the LMC kinematic center using PMs of RC stars. Further, the inclination of the disk is also different (taken 37° in B22, inferred to be 23° from model fitting in C22). These differences arise because the LMC's center depends on the stellar population used, and whether PM information is used in computing the center or not (Rathore et al. 2025c). To ensure the discrepancy in the LMC's center and disk inclination does not affect our statistical framework, we calculate the surrounding RC velocities in the C22 adopted coordinate frame, and then transform all velocities back to PMs and RVs before performing any statistical computations. Since the definition of the PMs and RVs is LMC frame independent, our conclusions are robust to the choice of reference frame.

We now briefly describe the C22 kinematic model in their adopted coordinate system (here referred as $\tilde{r}, \tilde{\phi}, \tilde{z}$ to distinguish it from the B22 coordinate system r, ϕ, z). Velocities in the r' and z' direction are taken to be 0. The tangential velocity profile as a function of distance from the LMC center is given by

$$v(\tilde{r}) = \begin{cases} v_0 \left(\frac{\tilde{r}}{\tilde{r}_0} \right), & \tilde{r} < \tilde{r}_0 \\ v_0, & \tilde{r} > \tilde{r}_0 \end{cases} \quad (4)$$

This equation results in a velocity profile that increases linearly until the scale radius \tilde{r}_0 , after which it flattens to the constant value v_0 . All of v_0, \tilde{r}_0 and $\eta = \tilde{r}_0/d_{\text{LMC}}$ are inferred from model fitting to RC PMs.

We compute the model-based mean PMs and RVs for the surrounding stars at the GC locations by supplying the best-fit parameters in C22 to the velocity equations (eq. 1–36) in [van der Marel et al. \(2002\)](#). The computation of the PM dispersion at each GC location is detailed in section 3.3.2.

3.3. Constructing Statistical Metrics for Velocity Differences

The net PM difference between the GC and its surrounding stars is calculated as a 2D vector, with components $\Delta\mu_\alpha^*$ and $\Delta\mu_\delta$ for difference in RA (pre-corrected with $\cos\delta$) and DEC respectively. The net difference becomes:

$$\Delta_{\text{pm}} = \sqrt{\Delta\mu_\alpha^{*2} + \Delta\mu_\delta^2} \quad (5)$$

Let the error in Δ_{pm} be ϵ_{pm} and the intrinsic velocity dispersion of the surrounding stars be σ_{pm} . The calculation for ϵ_{pm} and σ_{pm} are different for data-obtained surrounding velocities (section 3.1) and model-obtained surrounding velocities (section 3.2), and are elaborated in the following subsections (section 3.3.1 and section 3.3.2).

We construct two metrics to check for the statistical significance of the PM difference (Δ_{pm}). We call these metrics Q_{err} and Q_{disp} , which are defined as:

$$Q_{\text{err}} = \frac{\Delta_{\text{pm}}}{\epsilon_{\text{pm}}} \quad (6)$$

$$Q_{\text{disp}} = \frac{\Delta_{\text{pm}}}{\sigma_{\text{pm}}} \quad (7)$$

Q_{err} quantifies how significant is the PM difference between a GC and its surrounding stars when accounting for the measurement error. Q_{disp} quantifies how significant the difference is when accounting for the intrinsic velocity dispersion at that location.

We outline three different scenarios for calculating Q_{err} and Q_{disp} for each GC, to ensure the best selection of GCs with a statistically significant velocity difference from its surroundings.

3.3.1. Using Gaia DR3 Measurements of the Surrounding Stars

Let $\epsilon_\alpha(\text{GC})$ and $\epsilon_\alpha(\text{surr})$ denote the PM errors in RA for the GC and the surrounding stars respectively. Let $\epsilon_\delta(\text{GC})$ and $\epsilon_\delta(\text{surr})$ denote the PM errors in DEC for the GC and the surrounding stars respectively. The errors for the GC [$\epsilon_\alpha(\text{GC})$ and $\epsilon_\delta(\text{GC})$] are obtained from the B22 catalogue, and the errors for the surrounding stars [$\epsilon_\alpha(\text{surr})$ and $\epsilon_\delta(\text{surr})$] are obtained with the computation in section 3.1. The final error in the net PM

difference (ϵ_{pm}) is calculated by a Gaussian error propagation as follows:

$$\epsilon_\alpha = \sqrt{\epsilon_\alpha(\text{GC})^2 + \epsilon_\alpha(\text{surr})^2} \quad (8)$$

$$\epsilon_\delta = \sqrt{\epsilon_\delta(\text{GC})^2 + \epsilon_\delta(\text{surr})^2} \quad (9)$$

$$\epsilon_{\text{pm}}^2 = \left(\frac{\Delta\mu_\alpha^*}{\Delta_{\text{pm}}}\right)^2 \epsilon_\alpha^2 + \left(\frac{\Delta\mu_\delta}{\Delta_{\text{pm}}}\right)^2 \epsilon_\delta^2 \quad (10)$$

Since the radial density of stars drops sharply in GCs and the R_{in} used for the surrounding annulus is of the typical tidal radius value, we expect contamination from the GC stars in the surrounding sample to be minimum. This ensures the errors on the PMs of the GC population and the surrounding star population can be assumed to be nearly independent, justifying Gaussian propagation. The dispersion values (σ_{pm}) obtained in section 3.1 are directly used to compute Q_{disp} for each GC.

The aforementioned scenario of using the *Gaia* DR3 measurements of surrounding stars to compute the GC–surrounding PM differences is henceforth referred to as the “ M_{data} scenario”.

We note that in the above treatment, systematic errors in the *Gaia* PM measurements have not been considered. The systematic errors are spatially correlated (as shown in [Lindegren et al. 2021](#)). We have further verified the presence of this spatial correlation by examining the PM systematic error maps of the LMC field on an $8^\circ \times 8^\circ$ region (received from Paul McMillan, *priv. comm.*, see also Figure 17 of [Gaia Collaboration et al. 2018](#)). We do not expect the spatially correlated systematic errors to affect our statistical framework, as justified in the paragraph below.

The values reported for the GC PMs in the B22 catalogue are not corrected for the aforementioned systematic errors. Mathematically, if $\mu_\delta(\text{GC})$ is the truth value of the GC PM along the DEC direction, the value reported in B22 is actually $\mu_\delta(\text{GC}) + \epsilon_{\text{sys}}$, where ϵ_{sys} is the systematic error for μ_δ at the GC’s spatial location. Since the systematic error is spatially correlated at length scales $< 0.2^\circ$ (which is the maximum outer radius we use for the surrounding star selection), our method to find the PMs of surrounding stars (section 3.1) returns the value $\mu_\delta(\text{surr}) + \epsilon_{\text{sys}}$, where $\mu_\delta(\text{surr})$ is the truth value of the mean PM of the surrounding stars. When we compute the difference ($\Delta\mu_\delta$) between the GC PM and the surrounding star PM, the systematic term (ϵ_{sys}) cancels out. In this paragraph, we have used the DEC component just for illustration, but a similar reasoning applies to the RA component.

3.3.2. Using a 2D Kinematic Model for Surrounding Star Velocities

The velocity field of the surrounding stars at the GC coordinates are derived as given in section 3.2. In the model based approach, the error on the velocities of the surrounding stars is taken to be 0. Hence, the only contribution to ϵ_{pm} is from the GC's PM measurement errors, which are obtained by Gaussian error propagation from the RA and DEC components:

$$\epsilon_{\text{pm}}^2 = \left(\frac{\Delta\mu_\alpha^*}{\Delta_{\text{pm}}} \right)^2 \epsilon_\alpha(\text{GC})^2 + \left(\frac{\Delta\mu_\delta}{\Delta_{\text{pm}}} \right)^2 \epsilon_\delta(\text{GC})^2 \quad (11)$$

where the terms denote the same quantities as section 3.3.1. The above equation is used to calculate Q_{err} . A local velocity dispersion model (i.e. velocity dispersion as a function of r, ϕ, z) has not been developed for the LMC RC population in prior literature, and is currently beyond the scope of this work. However, to get an estimate of the velocity dispersion that we can use for our model driven approaches (outlined below), we utilize the velocity dispersion curve for the LMC red giant stars formulated in Vasiliev (2018). The coordinate reference frame in Vasiliev (2018) (adopted LMC center and disk inclination) is roughly the same as in B22, and the minor differences do not affect the overall conclusions of our analysis. In Vasiliev (2018), velocity dispersions are reported along the (r, ϕ) directions ($\sigma_{R,\phi}$) and along the z direction (σ_z) separately, as a function of distance from the LMC center (r).

To calculate the PM dispersion in the sky plane, we use the plane-of-sky projection of the two components ($\sigma_{R,\phi} \cdot \cos i$ and $\sigma_z \cdot \sin i$) and take their sum in quadrature:

$$\sigma_{\text{pm}}(r) = \sqrt{\sigma_{R,\phi}^2(r) \cos^2 i + \sigma_z^2(r) \sin^2 i} \quad (12)$$

where $i = 37.4^\circ$ is the inclination of the LMC disk with respect to our line-of-sight adopted in B22. Note that V18 do not provide a single value for the inclination but rather a range of $32^\circ - 35^\circ$. We have verified that this small range of inclinations does not affect our results.

Q_{disp} is calculated using eq. (12), and we refer to the scenario described in this subsection as the “ $M_{2\text{Dmodel}}$ scenario”.

3.3.3. Using a 3D Kinematic Model for the Surrounding Star Velocities

The C22 model provides the full 3D velocities for the surrounding stars at the GC's location. Since the B22 catalogue also reports the GC's own 3D velocity, we calculate the full 3D velocity difference (instead of just the PM difference), and call it $\Delta_{3\text{D}}$. As mentioned in section 3.2, all GC and surrounding velocities are converted to PMs and RVs before computing differences and statistical metrics. A conversion factor of $1 \text{ mas yr}^{-1} = 237.21$

km/s at 50 kpc (Pietrzyński et al. 2013) is used to convert RVs in km s^{-1} to mas yr^{-1} to match the units of PM. Similar to section 3.3.2, the error $\epsilon_{3\text{D}}$ is calculated using Gaussian propagation from the errors in the GC's PM and RV. The errors in the surrounding velocities calculated from the C22 model are taken to be 0.

Velocity dispersion $\sigma_{3\text{D}}$ is computed using the red giant model in Vasiliev (2018, hereafter V18). For the full 3D velocity, we take the sum of $\sigma_{R,\phi}$ and σ_z in quadrature without the inclination factor.

$$\sigma_{3\text{D}}(r) = \sqrt{\sigma_{R,\phi}^2(r) + \sigma_z^2(r)} \quad (13)$$

Q_{err} and Q_{disp} are calculated (similar to § 3.3) as follows:

$$Q_{\text{err}} = \frac{\Delta_{3\text{D}}}{\epsilon_{3\text{D}}} \quad (14)$$

$$Q_{\text{disp}} = \frac{\Delta_{3\text{D}}}{\sigma_{3\text{D}}} \quad (15)$$

The scenario described in this subsection is henceforth referred to as the “ $M_{3\text{Dmodel}}$ scenario”.

To summarize our statistical framework, we have Q_{err} and Q_{disp} values under three different scenarios -

- a) *M_{data} scenario*: Using the PM difference between the GC (taken from B22) and the surrounding RC stars (computed using *Gaia* DR3). The velocity dispersions of the surrounding stars are also computed using the *Gaia* DR3 measurements.
- b) *$M_{2\text{Dmodel}}$ scenario*: Using the PM difference between the GC (taken from B22) and the surrounding RC stars (computed using the C22 model). The in-plane velocity dispersions of the surrounding stars is computed from the red giant model of V18.
- c) *$M_{3\text{Dmodel}}$ scenario*: Using the 3D velocity differences between GC (taken from B22) and the surrounding red clump stars (computed using C22 model). The 3-D velocity dispersions of the surrounding stars is computed from the red giant model of V18.

4. A CATALOGUE OF OUTLYING LMC GLOBULAR CLUSTERS

We select GCs that have $Q_{\text{err}} > 3$ (velocity difference between the GC and surrounding stars is inconsistent with 0 at $> 3\sigma$ level under measurement errors) and $Q_{\text{disp}} > 1$ (velocity difference between the GC and surrounding stars is greater than the velocity dispersion of the surrounding stars).

The sample of GCs satisfying the above criteria are different under the three scenarios considered (M_{data} ,

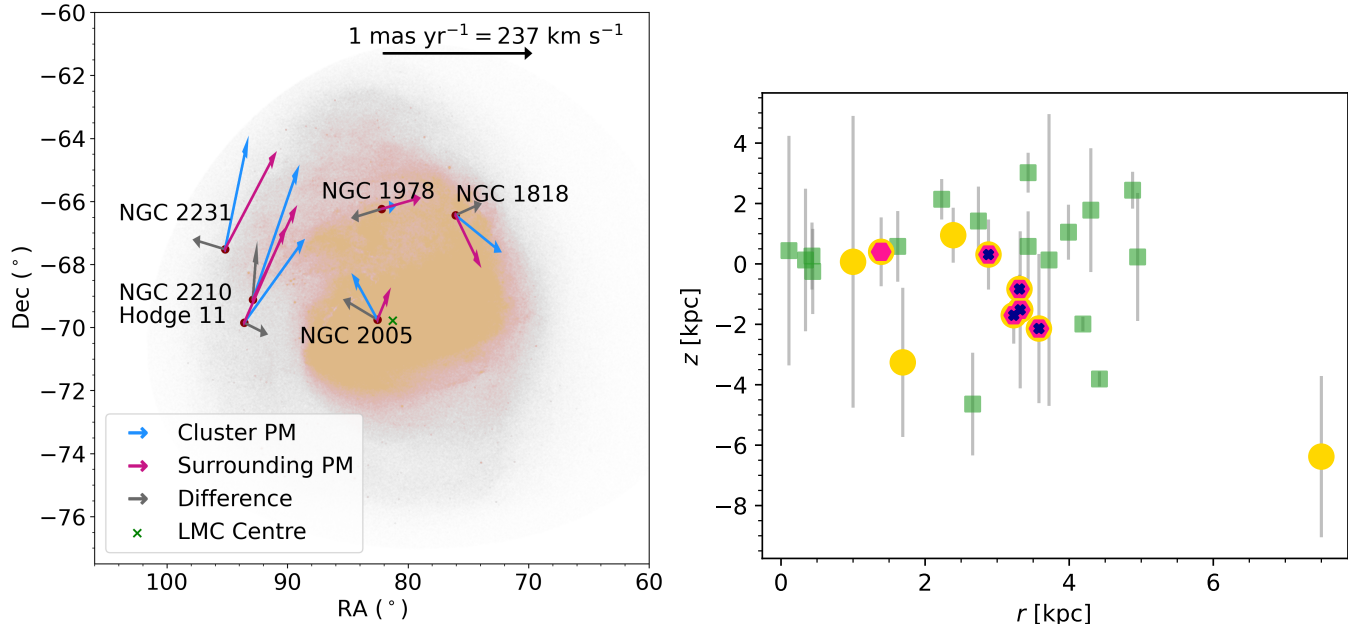


Figure 2. *Left panel:* PM difference vectors (in grey) between the GC (in blue) and their surrounding RC stars (in magenta). Only the 6 GCs having a statistically significant difference with their surrounding stars under both *Gaia* DR3 data (M_{data}) and the RC kinematic model ($M_{2\text{Dmodel}}$) are shown (see Table 2). These GCs are overlaid on a background of LMC stars obtained from *Gaia* DR3. The surrounding field PMs clearly show the expected rotational pattern. While the directions of the velocity differences do not show any trend, 5 of the 6 GCs are located at similar distances ($\sim 3 - 4$ kpc) from the LMC photometric center (marked with a green cross). *Right panel:* Distribution of the GCs in the r - z space of the LMC-centric coordinate system. Green squares are all the non-outlier GCs. Outlying GCs under $M_{3\text{Dmodel}}$, $M_{2\text{Dmodel}}$, and M_{data} , are marked with yellow circles, pink hexagons and blue crosses respectively. Grey errorbars denote the $1 - \sigma$ uncertainty in z . Uncertainties in r are negligible compared to the uncertainty in z . Consistent with the finding in the *left panel*, the high difference GCs under all three scenarios (marked with yellow, pink and blue) are clustered in the $r - z$ space. The 2D Kolmogorov-Smirnov test returns a p -value ≈ 0.01 for the hypothesis that both the set of outlier GCs and the set of remaining GCs were drawn from the same underlying distribution, indicating that their clustering is statistically significant.

$M_{2\text{Dmodel}}$ and $M_{3\text{Dmodel}}$). Importantly, small differences between a GC RV and the model-predicted RV for its surroundings, coupled with low uncertainties on the RV of the GC can increase Q_{err} and Q_{disp} under $M_{3\text{Dmodel}}$. As a result, the criteria defined in the above paragraph ($Q_{\text{err}} > 3$ and $Q_{\text{disp}} > 1$) flag about a third of the GC sample as kinematic outliers under the scenario $M_{3\text{Dmodel}}$.

Analyzing the statistical significance of the 2D velocity differences gives us more conservative results, in the sense that less number of GCs are flagged as outliers. $M_{2\text{Dmodel}}$ flags 6 GCs as kinematic outliers, out of which 5 are flagged in M_{data} as well. All of these 6 GCs under $M_{2\text{Dmodel}}$ were also flagged as outliers under $M_{3\text{Dmodel}}$. In general, it would be expected for the M_{data} or $M_{2\text{Dmodel}}$ scenarios to give more conservative results as compared to $M_{3\text{Dmodel}}$, since $M_{3\text{Dmodel}}$ picks out the GCs that may not have high PM differences but have high RV differences with respect to their surroundings.

The full set of results - GC PMs and RVs, data-derived PMs for the surroundings, model-derived velocities for the surroundings, and the values of Q_{err} and Q_{disp} un-

der M_{data} , $M_{2\text{Dmodel}}$ and $M_{3\text{Dmodel}}$ scenarios for all the LMC GCs considered in this study are given in Tables 1 and 2.

The PM vectors of the 6 GCs identified as outliers in Table 1 are plotted in Figure 2 *left panel*. The PM vectors of the surrounding stars as well as the PM difference vectors between the GC and the surroundings are also shown. We do not find any trend in the directions of the PM difference vectors across the 6 GCs. However, surprisingly, 5 out of 6 outlying GCs are located at a similar radial distance (3–4 kpc) from the LMC’s photometric center. Interestingly, [Olsen et al. \(2011\)](#) found a population of stars potentially accreted from the SMC also at a radius of ~ 3 kpc. We note that this is also approximately the radius where the rotation curve changes from rising to flat and could potentially contribute to artificial velocity residuals when comparing against the model ($M_{2\text{Dmodel}}$). However, this is unlikely to be the case since the GCs around 3–4 kpc are outliers selected by both M_{data} and $M_{2\text{Dmodel}}$ scenarios.

The distribution of the LMC GC sample in the $r - z$ space is visualized in Figure 2 *right panel*. Uncertainties

Name of GC	GC Proper Motion in RA [mas yr ⁻¹]	GC Proper Motion in Dec [mas yr ⁻¹]	Surrounding Proper Motion in RA [mas yr ⁻¹]	Surrounding Proper Motion in Dec [mas yr ⁻¹]	Proper Motion Difference $\Delta_0 \pm \epsilon$ [mas yr ⁻¹]	Velocity Dispersion σ_v [mas yr ⁻¹]	Q_{err}	Q_{disp}
NGC 1644	-0.151 ± 0.123	-0.679 ± 0.131	-0.108 ± 0.027	-0.633 ± 0.028	0.063 ± 0.13	0.12	0.485	0.528
NGC 1651	0.082 ± 0.178	-0.7 ± 0.158	0.094 ± 0.025	-0.638 ± 0.025	0.063 ± 0.161	0.155	0.392	0.407
NGC 1652	-0.076 ± 0.325	-1.042 ± 0.339	0.015 ± 0.025	-0.648 ± 0.025	0.405 ± 0.339	0.146	1.194	2.765
NGC 1756	0.0 ± 0.01	-0.424 ± 0.01	0.058 ± 0.025	-0.437 ± 0.025	0.059 ± 0.027	0.241	2.24	0.247
NGC 1783	-0.233 ± 0.043	-0.394 ± 0.05	-0.165 ± 0.025	-0.382 ± 0.025	0.069 ± 0.05	0.152	1.382	0.453
NGC 1786	0.094 ± 0.098	-0.321 ± 0.159	-0.061 ± 0.024	-0.347 ± 0.025	0.157 ± 0.103	0.19	1.522	0.825
NGC 1806	-0.002 ± 0.064	-0.418 ± 0.067	-0.051 ± 0.024	-0.326 ± 0.024	0.104 ± 0.071	0.219	1.477	0.476
NGC 1831	-0.178 ± 0.045	-0.376 ± 0.061	-0.197 ± 0.025	-0.295 ± 0.025	0.084 ± 0.065	0.133	1.279	0.628
NGC 1866	-0.292 ± 0.047	-0.182 ± 0.072	-0.233 ± 0.025	-0.193 ± 0.025	0.06 ± 0.054	0.149	1.114	0.404
NGC 1868	-0.24 ± 0.167	-0.173 ± 0.257	-0.197 ± 0.026	-0.211 ± 0.026	0.057 ± 0.213	0.139	0.269	0.413
NGC 1928	0.011 ± 0.01	-0.07 ± 0.01	-0.022 ± 0.027	0.009 ± 0.027	0.085 ± 0.029	0.453	2.954	0.188
NGC 1939	0.113 ± 0.01	-0.075 ± 0.01	0.043 ± 0.025	0.03 ± 0.025	0.126 ± 0.027	0.388	4.65	0.325
NGC 1987	0.164 ± 0.009	0.027 ± 0.009	0.138 ± 0.024	0.079 ± 0.024	0.058 ± 0.026	0.287	2.235	0.202
NGC 2108	-0.215 ± 0.01	0.365 ± 0.01	-0.208 ± 0.026	0.391 ± 0.026	0.027 ± 0.028	0.226	0.964	0.118
NGC 2159	-0.316 ± 0.075	0.509 ± 0.031	-0.264 ± 0.025	0.515 ± 0.025	0.052 ± 0.079	0.155	0.662	0.336
NGC 2162	-0.415 ± 0.084	0.472 ± 0.076	-0.33 ± 0.027	0.374 ± 0.027	0.13 ± 0.084	0.119	1.545	1.093
NGC 2173	0.081 ± 0.043	0.501 ± 0.031	0.012 ± 0.025	0.493 ± 0.025	0.069 ± 0.05	0.137	1.391	0.504
NGC 2190	0.028 ± 0.052	0.506 ± 0.056	0.014 ± 0.027	0.481 ± 0.027	0.029 ± 0.061	0.149	0.467	0.192
NGC 2209	0.029 ± 0.154	0.582 ± 0.171	-0.025 ± 0.026	0.573 ± 0.027	0.055 ± 0.157	0.097	0.348	0.56
Hodge 4	-0.227 ± 0.08	0.004 ± 0.09	-0.289 ± 0.025	0.078 ± 0.025	0.096 ± 0.09	0.168	1.071	0.573
NGC 1835	0.135 ± 0.013	-0.38 ± 0.024	0.055 ± 0.026	-0.255 ± 0.026	0.149 ± 0.033	0.323	4.448	0.46
NGC 1898	0.137 ± 0.017	-0.092 ± 0.02	0.045 ± 0.026	-0.071 ± 0.026	0.094 ± 0.031	0.444	3.045	0.212
NGC 1916	-0.031 ± 0.055	0.119 ± 0.083	-0.022 ± 0.027	-0.027 ± 0.027	0.146 ± 0.087	0.464	1.678	0.315
NGC 2005	0.144 ± 0.044	0.301 ± 0.063	-0.059 ± 0.025	0.166 ± 0.025	0.243 ± 0.057	0.424	4.304	0.574
NGC 2019	0.044 ± 0.034	0.038 ± 0.075	-0.039 ± 0.026	0.194 ± 0.026	0.177 ± 0.073	0.42	2.43	0.421
NGC 1818	-0.333 ± 0.032	-0.249 ± 0.048	-0.167 ± 0.025	-0.321 ± 0.025	0.181 ± 0.043	0.177	4.217	1.019
NGC 1978	-0.074 ± 0.048	0.026 ± 0.058	-0.277 ± 0.025	0.085 ± 0.025	0.211 ± 0.055	0.185	3.854	1.14
NGC 2210	-0.309 ± 0.066	0.971 ± 0.025	-0.288 ± 0.025	0.671 ± 0.025	0.301 ± 0.035	0.127	8.482	2.37
NGC 2231	-0.158 ± 0.046	0.77 ± 0.114	-0.366 ± 0.025	0.706 ± 0.025	0.217 ± 0.061	0.114	3.585	1.907
Hodge 11	-0.393 ± 0.034	0.614 ± 0.049	-0.267 ± 0.025	0.685 ± 0.026	0.145 ± 0.046	0.14	3.165	1.034

Table 1. Comparison of PMs of the GCs (taken from [Bennet et al. 2022](#)) against the average PMs of the surrounding stars (computed from *Gaia* DR3 data using a likelihood maximization scheme, [Vasiliev 2019a](#)). All PMs are in the LMC center-of-mass frame from C22 ($\mu_{\alpha, \text{COM}}^* = 1.859$, $\mu_{\delta, \text{COM}} = 0.375$). The last five GCs have a statistically significantly different PM from the surrounding stars, with $Q_{err} > 3$ (velocity difference is at least 3σ with respect to measurement uncertainties) and $Q_{disp} > 1$ (velocity difference is greater than the velocity dispersion). For each GC named in the first column, we provide its PM components (columns 2 and 3), as well as the average PM components of its surrounding stars (columns 4 and 5). The PM difference between the GC and surrounding stars and the error in that difference is given in column 6. PM dispersion of the surrounding stars is given in column 7. Our statistical metrics (Q_{err} and Q_{disp}) for evaluating the significance of the PM difference between the GC and its surrounding stars are given in columns 8 and 9. Derivation of PMs and dispersions of the surrounding stars corresponding to each GC has been elucidated in section 2.2.

in z are taken to be the same as the distance uncertainties given in Table 1 of B22. This is justified since the LMC is approximately face-on. Uncertainties in r are negligible as compared to the uncertainty in z . The 5 outliers under the scenario M_{data} are found to cluster in the $r - z$ space, consistent with Figure 2 *left panel*. We perform the 2D Kolmogorov-Smirnov (KS) test ([Peacock 1983](#); [Fasano & Franceschini 1987](#)) on the full distribution of (r, z) v/s the (r, z) of the 5 kinematic out-

liers flagged under all three ϵ scenarios. We use the public code NDTEST⁴. The p value for the two sets being drawn from the same underlying distribution is 0.046, indicating that the kinematically outlying set has a statistically different distribution of (r, z) values as compared the full population of GCs. This further drops to $p = 0.011$ if

⁴ Written by Zhaozhou Li, <https://github.com/syrte/ndtest>

Name of GC	GC Radial Velocity [km s ⁻¹]	Surr. Model PM in RA [mas yr ⁻¹]	Surr. Model PM in Dec [mas yr ⁻¹]	Surr. Model RV (km/s) [km s ⁻¹]	Surr. Model Dispersion [mas yr ⁻¹]	2D Model Q _{err}	2D Model Q _{disp}	3D Model Q _{err}	3D Model Q _{disp}
NGC 1644	-18.0±5.0	-0.108	-0.641	-6.755	0.119	0.454	0.734	0.759	0.629
NGC 1651	-35.8±2.3	0.118	-0.637	-33.876	0.178	0.445	0.592	0.451	0.411
NGC 1652	11.7±1.3	0.005	-0.662	-17.871	0.149	1.149	3.875	1.266	2.735
NGC 1756	...	0.042	-0.425	-11.857	...	4.174	1.0
NGC 1783	27.6±9.9	-0.189	-0.39	18.217	0.135	1.019	0.486	1.388	0.437
NGC 1786	16.0±5.0	-0.068	-0.372	3.504	0.164	1.616	1.511	1.768	1.083
NGC 1831	16.0±5.0	-0.224	-0.279	26.363	0.119	1.85	1.381	2.133	0.983
NGC 1866	34.4±0.4	-0.252	-0.17	30.657	0.14	0.842	0.446	0.958	0.32
NGC 1868	19.0±3.0	-0.246	-0.169	34.618	0.128	0.034	0.08	2.791	0.521
NGC 1898	-54.0±5.0	0.04	-0.075	-5.615	0.24	5.748	0.579	11.113	0.944
NGC 1916	14.0±5.0	0.018	-0.048	-2.527	0.245	2.145	1.008	2.473	0.766
NGC 1928	-14.4±12.8	0.017	-0.011	-2.255	0.24	5.882	0.347	2.152	0.326
NGC 1939	-5.2±7.4	0.05	0.0	-6.513	0.25	9.807	0.555	9.697	0.393
NGC 1987	...	0.09	0.096	-11.866	...	11.199	1.0
NGC 2019	16.6±2.3	0.033	0.164	-4.683	0.197	1.696	0.928	2.53	0.788
NGC 2108	...	-0.085	0.342	8.711	...	13.185	1.0
NGC 2162	38.0±3.5	-0.351	0.38	62.256	0.131	1.428	1.282	2.577	1.158
NGC 2173	-26.6±0.7	0.075	0.522	-18.468	0.149	0.695	0.221	2.353	0.275
NGC 2209	-9.0±3.0	0.015	0.616	-16.272	0.129	0.217	0.427	0.367	0.37
Hodge 4	46.8±1.9	-0.292	0.092	42.318	0.168	1.268	0.959	1.304	0.665
NGC 1806	-39.0±5.0	-0.054	-0.321	2.956	0.173	1.663	0.931	5.298	1.209
NGC 1835	-76.0±5.0	0.044	-0.26	-8.385	0.22	7.3	0.973	15.373	1.468
NGC 2159	-211.0±30.0	-0.196	0.548	18.157	0.196	1.754	0.925	7.749	4.983
NGC 2190	-4.0±3.0	0.07	0.517	-24.092	0.088	0.827	0.735	3.605	1.08
NGC 1818	47.0±4.0	-0.169	-0.307	17.739	0.15	5.092	1.723	7.218	1.423
NGC 1978	28.0±2.5	-0.245	0.077	31.198	0.16	3.656	1.642	3.677	1.121
NGC 2005	6.0±5.0	0.01	0.134	-1.417	0.205	3.803	1.491	3.878	1.058
NGC 2210	79.0±5.0	-0.227	0.696	19.974	0.152	9.414	2.807	14.13	2.497
NGC 2231	13.6±1.4	-0.343	0.715	41.859	0.143	3.523	2.004	4.855	1.592
Hodge 11	-18.9±1.0	-0.197	0.728	14.801	0.15	5.909	2.247	8.218	1.788

Table 2. Comparison of the GC velocities (taken from B22) with the average surrounding RC stars’ velocities computed using the C22 kinematic model. All PMs and RVs are in the LMC center-of-mass frame from C22 ($\mu_{\alpha, \text{COM}}^* = 1.859$, $\mu_{\delta, \text{COM}} = 0.375$, $\text{RV}_{\text{COM}} = 264.05$ km s⁻¹). The last 6 GCs have a significantly different PM and 3D velocity as compared to the model predictions. The preceding 4 GCs have a significantly different 3D velocity as compared to the model prediction, but they do not have a significantly different PM. For each GC in column 1, we list its RV in column 2, followed by the surrounding star model velocities and velocity dispersions in columns 3–6. The statistical metrics for evaluating the significance of the 2D and 3D velocity differences between a GC and its surrounding stars are given in columns 7–10. Velocity dispersions are computed using the 3D velocities, and are quoted in mas yr⁻¹ for easy comparison (at LMC distance, 1 mas yr⁻¹ = 237.2 km s⁻¹). NGC 1756, 1987 and 2108 did not have RV data or precise LoS distances calculated in B22, so their entries are empty in some of the columns. Derivation of PMs and RVs of a GC’s surrounding stars has been elucidated in section 3.3.3.

we compare the outlier cluster set against the non-outlier cluster set only (instead of the full population).

We emphasize the necessity of using both the metrics Q_{err} and Q_{disp} for selecting a reliable set of high-difference GCs. High velocity differences between the GCs and their surrounding stars are found in the LMC’s central regions. However, the LMC’s central region has intrinsically high PM dispersions, and hence these GCs

cannot be called outlying unless the velocity differences exceed the local velocity dispersion. Similarly, GCs at large radii ($r \gtrsim 5$ kpc) have high velocity differences, but they are located in sparser regions of LMC resulting in higher uncertainties on the mean PMs of surrounding stars. Hence, these GCs cannot be called outlying unless the velocity difference is statistically significant over the PM uncertainties. It is necessary to use both

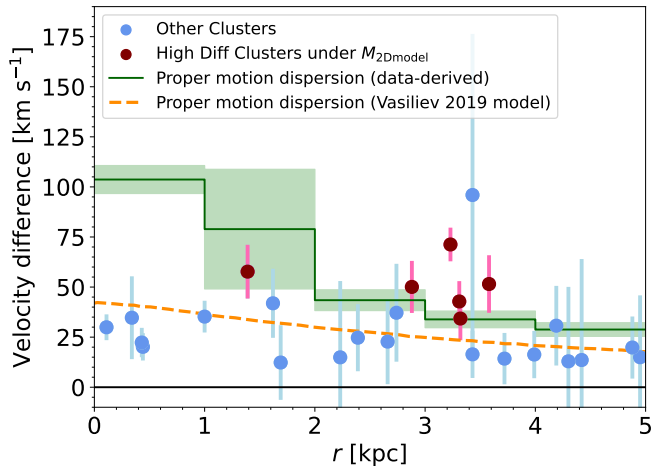


Figure 3. GC velocity differences are compared with the velocity dispersion of the surrounding stars, as a function of the radial coordinate (R). The velocity dispersions are obtained in two ways - using *Gaia* DR3 data (green solid line) and using the RGB model of Vasiliev (2018) (orange dashed line). The 6 high difference GCs identified in Table 2 are marked in pink and the remaining GCs are marked in blue. $1 - \sigma$ errorbars on the velocity differences are also shown. The green band denotes the standard deviation of the velocity dispersion values in each distance bin (1–2 kpc, 2–3 kpc and so on), with the average velocity dispersion for that distance bin marked with the solid green line.

the metrics, Q_{err} and Q_{disp} , for carefully evaluating the significance of the GC velocity differences.

As a consistency check of our PM dispersion calculations of the surrounding stars with *Gaia* DR3 data (section 2.2.1), we compare the data-derived RC dispersions with the red giant based dispersion model of V18. This comparison is shown in Figure 3. We also plot the PM difference (along with errors) between the GC and its surroundings for the entire sample of GCs utilized in this work. The mean RC PM dispersions calculated with *Gaia* DR3 data are systematically higher as compared to the red giant model based dispersion curve. Although, for $r > 2$ kpc, this discrepancy is within the $3 - \sigma$ uncertainty of the data-derived dispersions. Note that the area over which we compute the RC PM dispersion (a circle of radius $\approx 0.15^\circ$) is larger than that used in V18 (a square of side 0.2°). Hence, there is a higher physical spread of velocities in our selected regions as compared to the spatial bins used in V18, which can partly account for the differences in the two dispersions for $r > 2$ kpc. The mean discrepancy between the two dispersions is much larger in the LMC’s inner 2 kpc, wherein the data derived dispersions are a factor of 2-3 larger than the model derived dispersions. The large discrepancy can be attributed to the high stellar crowding in the LMC’s inner regions (Rathore et al. 2025c). Indeed, the $1 - \sigma$

errorbar on the data derived dispersion is $\approx 25 \text{ km s}^{-1}$, which would make the data derived dispersions consistent with the model derived ones at the $2 - \sigma$ level. The data derived dispersions in the LMC’s inner 1 kpc are likely not reliable due to severe crowding. This further emphasizes the need to compare the GC velocity differences with both the data derived and the model derived PM differences, for identifying a sample of GCs that are truly kinematically outlying.

5. DISCUSSION

We have developed a statistical framework to select LMC GCs that are kinematically distinct from their surrounding LMC disk stars. We find five GCs (NGC 1818, NGC 1978, NGC 2210, NGC 2231 and Hodge 11) that have velocities that are significantly different from both data-derived and model-derived 2D and 3D velocities of the surrounding stars. One more GC (NGC 2005) has a significantly different velocity from only the model-derived 2D and 3D velocities of the surroundings. Four others (NGC 1806, NGC 1835, NGC 2159 and NGC 2190) have a significant differences only in the line-of-sight component of their velocity, and not their PM component. Next: (i) we place our results in the context of some previous studies on the LMC GCs; (ii) examine the dependence of the velocity differences on the age of GCs; (iii) investigate the reliability of the GC sample as a tracer of the LMC’s mass; (iv) assess the limitations of our analysis and prospects for the future.

5.1. Previous Investigations of Our Outlying GCs

Utilizing the full 3D velocity information ($M_{3\text{Dmodel}}$) yields 10 kinematic outliers. Of these, 4 are not outliers in the PM space, implying that they are outliers in the LoS velocity only. Of these four, NGC 2159 was also analyzed by Bennet et al. (2022) as a potential outlier based on its anomalous LoS velocity and discrepancy with the LMC’s average rotational field.

We note that three of the four GCs that are outliers only in the LoS velocity (NGC 1835, NGC 2159, NGC 2190) have RV estimates based on only a few (~ 5) member stars (Baird & Flower 1986; Olszewski et al. 1991; Sharma et al. 2010). Hence, the RV measurements for these GCs may not be very robust, and additional spectroscopic follow up is necessary. In this subsection, we only focus on the remaining 6 GCs, which are kinematic outliers in the PM space as well. We investigate previous works to find further evidence of anomalous behavior of these GCs.

NGC 1978 is a globular cluster with highly elliptical isodensity curves ($\epsilon \approx 0.30$, Mucciarelli et al. 2007), quite unlike most MW GCs (mean ellipticity ≈ 0.07 ,

and typical values between 0 and 0.15, Goodwin 1997) and lies at the upper end of the ellipticity range of other LMC GCs (0.05–0.30, with a mean ≈ 0.14 , Goodwin 1997). In general, LMC GCs have higher ellipticities as compared to the MW GCs. This is due to a weaker tidal field of the LMC compared to the MW, where in the former case the original triaxial structure of the GCs is preserved (Goodwin 1997 and references therein). However, the ellipticity of NGC 1978 is abnormally high. Ferraro et al. (2006) showed that such high ellipticities *cannot* be achieved with mergers of two GCs or even two progenitor molecular clouds, which makes the high ellipticity of NGC 1978 quite intriguing.

The peculiar shape of NGC 1978, combined with the large PM difference with the surroundings, suggests that the GC might have been born in a different environment. We propose that the anomalous kinematics and extra high ellipticity of NGC 1978 makes it a promising candidate of having been originally formed in a dwarf galaxy with a lesser tidal field strength as compared to the LMC. If the GC was accreted into the LMC much later, the LMC’s tidal forces would not have enough time to alter the shape of the GC.

In a recent study by Mucciarelli et al. (2021), NGC 2005 was found to have distinct chemical abundance patterns compared to other LMC GCs of similar metallicity, suggesting it originated in a different environment. Using chemical evolution models, they concluded that NGC 2005’s progenitor was likely a low-mass dwarf spheroidal galaxy with inefficient star formation. NGC 2005 ending up as a kinematic outlier in our framework lends further credence to this GC having an external origin.

B22 found that the speed of NGC 2210 relative to the LMC is likely larger than the LMC escape speed (see also Figure 1). NGC 2210 is an old GC (age > 8 Gyr, Olszewski et al. 1996), which shows multiple horizontal branches in its CMD (Gilligan et al. 2019, 2020). Multiple populations are typically seen in cores of accreted dwarf galaxies as shown in Helmi (2008), and such cores are likely progenitors of several MW GCs (Massari et al. 2019; Pfeffer et al. 2021; Belokurov & Kravtsov 2024). Hence, it is likely that NGC 2210 is not a LMC GC, and instead is a MW GC that happens to be near the LMC.

Apart from NGC 2210, Gilligan et al. (2019) observed that Hodge 11 is the only other LMC GC with multiple horizontal branches. Further, both NGC 2210 and Hodge 11 have the most heavily populated blue-straggler branch among the very old GCs (age > 12 Gyr) studied by Wagner-Kaiser et al. (2017). However, the relative speed of Hodge 11 with respect to the LMC suggests that it is bound to the LMC, unlike NGC 2210.

Further investigations of Hodge 11 are required, as its unique characteristics — being kinematically peculiar within the LMC disk and comparable in age to the oldest, metal-poor GCs in the MW — make it an ideal target to investigate the origin of the earliest GCs in LMC-mass galaxies.

5.2. Dependence of GC Kinematic Differences on Age

As mentioned previously, the LMC GC population has a mix of ages, including young GCs (age < 0.5 Gyr), intermediate age GCs ($0.5 \text{ Gyr} \leq \text{age} \leq 4.0$ Gyr) and old GCs (age $\gtrsim 10$ Gyr). Our model and data-driven estimates of the surrounding star PMs and RVs is derived using the RC population, which is dominated by ages of ~ 2 Gyr (Girardi 2016). We therefore expect kinematic differences between a GC and its surrounding stars to also arise due to the different epochs in the LMC’s evolution at which the GC and surrounding RC populations formed. The goal of this subsection is to understand to what extent are the kinematic differences of the GC population and the surrounding stars correlate with the GC ages.

A literature compilation of the ages of the GC sample analysed in this work are given in Table 3. We note that there are no GCs in the age range of 4–10 Gyr, which is well-known as an age gap in the LMC GC system (Olszewski et al. 1991; Bekki et al. 2004; Piatti 2022). In Figure 4 *left panel*, we plot: (i) the average and standard deviation of the PM difference of all the young, intermediate and old GCs considered in this work; and (ii) the PM difference as a function of age for the 6 outlying GCs identified under the $M_{2D\text{model}}$ scenario. There seems to be a slight mean trend of increasing PM difference as we go from young to intermediate to old GCs. However, given the size of the $1 - \sigma$ scatter, this trend is not statistically significant. For each age category, we create 10000 mock values of the PM difference by sampling from a Gaussian with a mean at the mean PM difference observed for that age category, and standard deviation equal to the $1 - \sigma$ scatter. We compute the Spearman correlation coefficient between the age and the PM difference for all 10000 realizations, and find its value to be $\rho = 0.42 \pm 0.54$, indicating that the correlation is consistent with 0. Further, no significant correlation is evident between the PM difference and ages of only the 6 outlying GCs (Spearman correlation coefficient = 0.23). In Figure 4, *middle* and *right* panels show the dependence of the statistical metrics Q_{err} and Q_{disp} on the GC ages. No correlation is evident between the value of these metrics and GC ages; neither for the outlier sample nor for the three age based GC categories.

Hence, the kinematic differences of the outlying GC population and the surrounding stars cannot be explained by GC age differences alone.

Further, ages for the 5 GCs flagged as outliers under the M_{data} scenario are: 2 Gyr for NGC 1978 (Narloch et al. 2022), > 10 Gyr for NGC 2210 and Hodge 11 (Sagar & Pandey 1989; Johnson et al. 1999; Wagner-Kaiser et al. 2017), 40 Myr for NGC 1818 from (Marino et al. 2018), ~ 13 Gyr for NGC 2005 (Olsen et al. 1998) and 1.6 Gyr for NGC 2231 (Piatti et al. 2014). There is no evidence of clustering in ages of these kinematically outlying GCs. We note that NGC 1818 is a very young GC. Hence, it is possible that the kinematics of NGC 1818 is similar to its parent gas cloud, which could explain why its velocity is different from the surrounding stars.

5.3. Implications for LMC Mass Estimate

Precise determination of the LMC’s mass, particularly the dark matter (DM) contribution, is important for several purposes, like - identifying LMC’s satellite galaxies (e.g. Patel et al. 2020), constraining the LMC-SMC interaction history (e.g. Besla et al. 2012; Kallivayalil et al. 2013; Patel et al. 2020; Jiménez-Arranz et al. 2024), placing the LMC-MW system in a cosmological context (e.g. Besla et al. 2018; Chamberlain et al. 2024; Arora et al. 2025), and ultimately, using the LMC as a testbed for DM particle physics (e.g. Foote et al. 2023, 2026).

Watkins et al. (2024) determined the mass profile of the LMC using the system of GCs in the B22 catalog. The tracer mass estimator (TME) used in their work is:

$$M(< r_{\text{max}}) = \frac{\alpha + \gamma - 2\beta}{G(3 - 2\beta)} \cdot r_{\text{max}}^{1-\alpha} \langle v^2 r^\alpha \rangle \quad (16)$$

Here G is the gravitational constant, r and v^2 are the radial distance in the LMC-centric cylindrical coordinates (r, ϕ, z) and the total velocity modulus squared respectively. $\langle \rangle$ denotes the average taken over the full tracer sample. γ is the power-law index for the radial distribution function of the GCs, β is the velocity anisotropy in the GCs and α is the power-law index that can be assumed to describe the gravitational potential over the range of r that is spanned by the cluster sample.

Watkins et al. (2024) assumed that the kinematics of their GC sample was an ideal tracer of the underlying gravitational potential. However, we have shown that a significant subset of the LMC GCs are kinematically outlying. Such outlying GCs may not be suitable tracers of the LMC’s mass. In this subsection, we investigate the effect of including or removing the kinematically outlying GCs on the LMC’s mass estimate.

We re-calculate the LMC’s TME for three GC samples

- 1) Using the full sample used in our analysis
- 2) The sample obtained after removing the 2D kinematic outliers
- 3) The sample obtained after removing the 3D kinematic outliers

Note that our full sample does not correspond to the full sample in B22 catalogue, since we removed many GCs that do not have PM and RV measurements. We newly include three GCs (NGC 1466, NGC 1841, Reticulum) that were not included in our velocity difference analysis because their surrounding star PMs could not be reliably estimated due to insufficient counts in the surrounding annuli. We also include NGC 2210 and NGC 2159 (not used by Watkins et al. 2024), as these are part of the kinematic outlier sets.

Therefore, the values of α, β, γ obtained by Watkins et al. (2024) would not be exactly the same for our sample. Re-evaluating these constants for our three samples is beyond the scope of this work. Moreover, evaluating the LMC’s mass precisely using the GC sample is not the focus of this work. Instead, we seek to determine how much the TME changes when the outlying GCs are removed. We use the same values of α, β, γ as derived by Watkins et al. (2024) for all three GC samples.

The maximum radius in our sample (i.e. the radius for the enclosed mass estimate) is $R_{\text{max}} = 11.59$ kpc. The TME inferred enclosed mass within R_{max} is $4.99 \times 10^{10} M_\odot$ for the full GC sample. Next, we remove the five GCs flagged as kinematic outliers in all three of M_{data} , $M_{2\text{Dmodel}}$ and $M_{3\text{Dmodel}}$, and recalculate the mass with the remaining GCs. The enclosed mass within R_{max} is $4.17 \times 10^{10} M_\odot$. Hence, the enclosed mass changes by 16% when the 2-D kinematic outliers are removed.

We ascertain the statistical significance of the change in enclosed mass through a bootstrapping procedure. We create 1000 realizations of GC sets with 5 random GCs removed from the full sample in each case, and recalculate the TME with the new sets. The resulting mass distribution consists of estimates with a mean of $4.97 \times 10^{10} M_\odot$, almost equal to the mass estimate from the full sample, as expected. The estimate with the 5 outliers removed ($4.17 \times 10^{10} M_\odot$) is $\approx 2\sigma$ away from this mean, where σ is the standard deviation of the mass distribution of bootstrapped realizations. The distribution of the bootstrapped realizations is approximately Gaussian, as shown in Figure 5 *left panel*.

Next, we remove the 6 GCs flagged as outliers in $M_{2\text{Dmodel}}$ and $M_{3\text{Dmodel}}$ from the full sample, and obtain a TME inferred enclosed mass within R_{max} of $4.24 \times 10^{10} M_\odot$. This new TME is different from the TME of the full sample by 15%. Repeating the bootstrapping

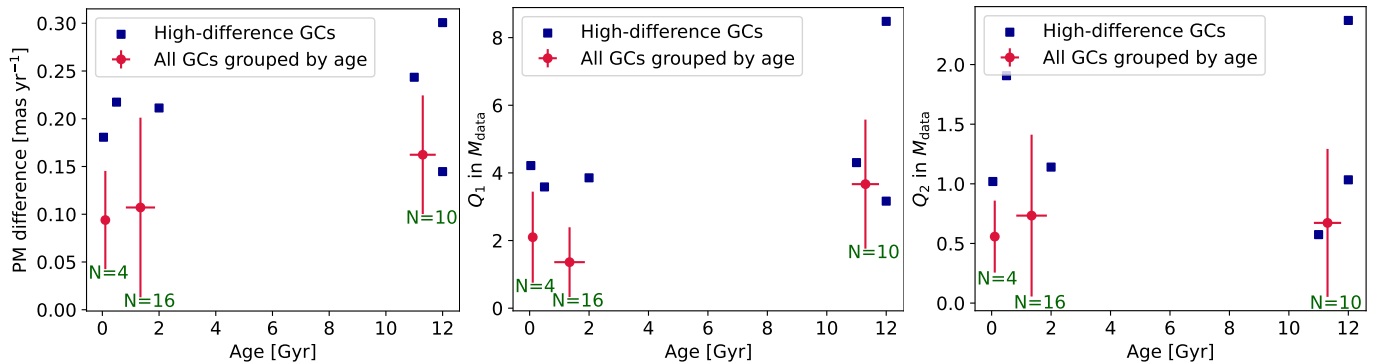


Figure 4. Dependence of the kinematic differences between the LMC GC population and their surrounding stars on the GC ages. The red points correspond to the entire GC sample analyzed in this work, categorized into young GCs (age < 0.5 Gyr, 4 in number), intermediate age GCs ($0.5 \text{ Gyr} \leq \text{age} \leq 4$ Gyr, 16 in number) and old GCs (age $\gtrsim 10$ Gyr, 10 in number). The blue squares denote the 6 outliers in the $M_{2\text{Dmodel}}$ scenario. *Left panel* shows the PM difference between the GC and surrounding stars as a function of GC age. When the entire GC sample is considered, there is a slight mean trend of older GCs having higher kinematic differences. However, given the standard deviation of the PM difference in each age group, this trend is not statistically significant. Further, no correlation is evident between the PM difference and age of the 6 outlying GCs. There is no evidence of the statistical metrics Q_{err} and Q_{disp} having a statistically significant dependence on GC age (*middle panel* and *right panel* respectively).

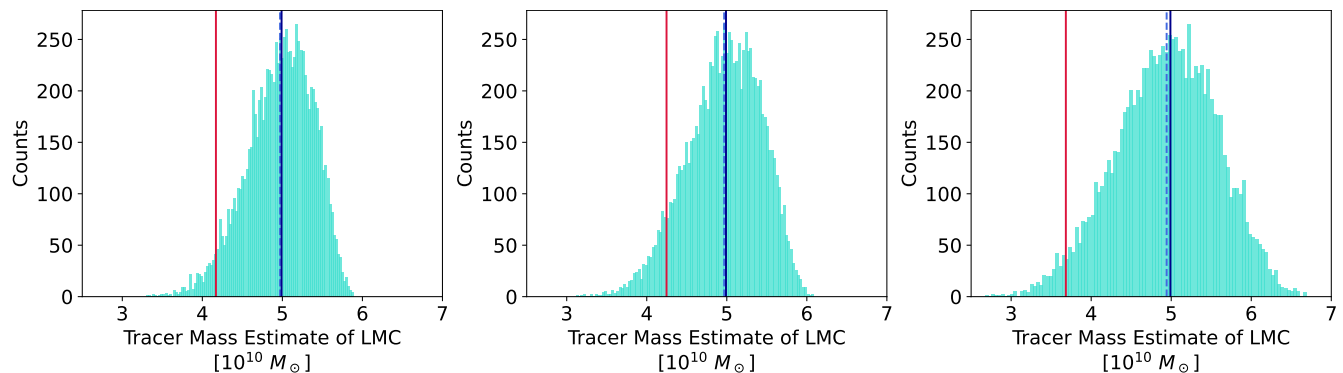


Figure 5. The GC based LMC tracer mass estimate (TME) with the full GC sample (solid blue line) v/s the estimate obtained by removing the outlier GCs flagged by M_{data} , $M_{2\text{Dmodel}}$ and $M_{3\text{Dmodel}}$ (solid red line in the *left*, *middle* and *right* panel respectively). The turquoise histogram depicts the TME distribution of the bootstrapped realizations obtained by randomly removing the same number of GCs as the outlying GCs and using only the remaining sample. The mean of the bootstrapped realizations (dashed blue line) is close to the full sample estimate as expected. We find that the kinematically outlying LMC GCs can bias the TME by as large as 30%.

analysis yields a statistical significance $\approx 1.65\sigma$ for this difference. The distribution of the bootstrapped realizations is approximately Gaussian, as shown in Figure 5 *middle panel*.

Finally, we remove the 10 GCs found to be outliers under $M_{3\text{Dmodel}}$ from the full sample, and obtain a TME inferred enclosed mass within R_{max} of $3.63 \times 10^{10} M_{\odot}$. This new TME is different from the TME of the full sample by $\approx 30\%$. Repeating the bootstrapping analysis yields a statistical significance of $\approx 2\sigma$ for this difference. The distribution of the bootstrapped realizations is approximately Gaussian, as shown in Figure 5 *right panel*.

To summarize, we find that including or excluding the kinematically outlying GCs can affect the LMC's en-

closed mass by 15% - 30%, depending on the outlier sample used. This bias will directly impact the LMC's DM content, since the baryonic mass profile is well measured (van der Marel et al. 2002; Kim et al. 2003; Olsen & Massey 2007). Further, the above bias is likely only a lower limit, since we have utilized the same value of α , β and γ (eq. 16) as Watkins et al. (2024). The values of these parameters can also change with the GC sample used, causing more uncertainty in the TME. Hence, caution must be exercised in using the LMC GC population to precisely determine the LMC's DM profile.

5.4. Limitations and Future Prospects

Our statistical framework for identifying kinematically outlying GCs takes into account the intrinsic velocity

dispersion of the LMC disk as well as statistical and systematic uncertainties in Gaia measurements. We do not explicitly account for crowding induced incompleteness in the LMC’s Gaia catalogs. Rathore et al. (2025c) showed that the completeness fraction for the RC population in the LMC’s inner 2 kpc is as low as 10%. This high incompleteness can affect our estimates of the average velocity and velocity dispersion of the surrounding star sample corresponding to GCs located in the LMC’s central region. However, we also present comparisons of the GC kinematics with model derived kinematics of the surrounding stars. Thus, our framework for identifying outlying GCs is not solely reliant on the Gaia measurements. Finally, most of the LMC GC’s are located at $R > 2$ kpc, where the completeness fraction is $> 90\%$ (Rathore et al. 2025c).

The LMC likely collided (impact parameter ~ 2 kpc) with the SMC ~ 100 Myr ago (Besla et al. 2016; Zivick et al. 2019; Choi et al. 2022; Rathore et al. 2025a; Jiménez-Arranz & Roca-Fàbrega 2025; Rathore et al. 2025b). Such a collision significantly affected the morphology and kinematics of the LMC bar and disk (see aforementioned references). This calls into question the validity of the C22 model for representing the LMC’s underlying velocity field. However, from Table 1 and 2, we find that NGC 2005 is the only GC which is a kinematic outlier when compared with the model derived surrounding star velocities, but is not outlying when compared with the data-derived surrounding star velocities. Hence, for a vast majority of the GCs, comparisons between the Gaia data and the C22 model are consistent. Hence, the usage of C22 model for representing the LMC’s underlying velocity field is justified. Further, incorporation of the surrounding star velocity dispersion in our statistical metrics accounts for the additional LMC disk heating due to the SMC collision.

To date, very few GCs have been identified in the SMC - with NGC 121 being the only confirmed member (Glatt et al. 2008), and Eridanus III and DES 1 being potential members (Conn et al. 2018). There is a reasonable likelihood that some of the kinematically outlying LMC GCs were in fact SMC GCs that have been accreted by the LMC during the close LMC-SMC interactions. Further, several of the kinematically outlying LMC GCs, despite having significantly different velocities, still share the same overall sense of rotation around the LMC center as the bulk of the stellar disk (Figure 2 *left panel*). While we are unable to provide a complete interpretation of this finding without dedicated dynamical simulations, we do speculate the possibility that several of these kinematically outlying GCs may have been accreted or disrupted by the same event, po-

tentially during a close encounter with the SMC. Future work involves a detailed comparison of metallicities, ages and chemical abundances of the kinematically outlying LMC GCs with stars in the SMC.

Finally, more accurate measurements of distances to individual GCs are needed to precisely constrain their position relative to the LMC disk, and potentially identify if any of the outlying GCs are actually positioned in the LMC halo and not the disk. This would provide a direct explanation for the kinematic mismatch if the surrounding disk stars used throughout this analysis only surround the GC in projection and not physically.

To conclude, the kinematically outlying LMC GCs that we have identified are fascinating targets for future spectroscopic follow-up observations, as understanding their origin and properties could be key to illuminating the LMC’s assembly history and DM halo properties.

6. CONCLUSIONS

We used *Gaia* DR3 astrometry for 30 LMC Globular Clusters (GCs) with the goal of identifying and characterizing GCs with outlying kinematics. We investigated the differences between GC kinematics (both Proper Motions and 3-D velocities) and the kinematics of stars in the LMC disk that surround the GC (surrounding stars). The surrounding stars were chosen to be the red clump (RC) stars residing in an annulus around a GC.

Proper Motion (PM) and 3-D velocity for each LMC GC was directly sourced from the catalog provided by Bennet et al. (2022). The average velocities and velocity dispersions of the surrounding stars were estimated in two ways: (i) directly using the Gaia DR3 measurements; (ii) using the C22 kinematic model. We calculated the mean PM and the associated uncertainty for the surrounding stars following the methodology of Vasiliev (2018).

We constructed two new statistical metrics to quantify the significance of differences in PM and 3D velocity with respect to the velocity measurement uncertainties and the intrinsic velocity dispersion of the surroundings (Q_{err} and Q_{disp} respectively, see section 3.3). We flagged all GCs with $Q_{\text{err}} > 3$ and $Q_{\text{disp}} > 1$ as outliers. Thus, GCs that show high values of both Q_{err} and Q_{disp} have velocity differences with respect to their surroundings that can neither be explained by the errors, nor by the intrinsic velocity dispersion. Further, the metrics Q_{err} and Q_{disp} are evaluated under three different scenarios: (i) considering data derived PMs and PM dispersions for the surrounding stars (M_{data} scenario); (ii) considering model derived PMs and PM dispersions for the surrounding stars ($M_{2\text{Dmodel}}$ scenario); and (iii) model derived 3-D velocities and 3-D velocity dispersions for

the surrounding stars ($M_{3Dmodel}$ scenario). Main results are as follows:

1. *Five GCs have statistically significant high PM difference relative to the surrounding stars.* These are NGC 1818, NGC 1978, NGC 2210, NGC 2231 and Hodge 11. We compared the GC PMs against the *Gaia* DR3-derived PMs and dispersions of their surrounding stars, as well as with the model derived PMs and 3-D velocities (and the dispersions). The aforementioned GCs have $Q_{err} > 3$ and $Q_{disp} > 1$ under all three scenarios - M_{data} , $M_{2Dmodel}$, and $M_{3Dmodel}$, as outlined in Tables 1 and 2.
2. *Ten GCs have high differences in 3D velocities.* Apart from the 5 GCs mentioned in the previous point, NGC 1806, NGC 1835, NGC 2005, NGC 2159 and NGC 2190 show statistically significant high velocity differences with respect to their surroundings when 3D velocity information is used.
3. *Kinematically outlying LMC GCs are clustered in the position space:* The 5 GCs that are outlying under all three (M_{data} , $M_{2Dmodel}$, and $M_{3Dmodel}$) scenarios reside at a radial distance of 3-4 kpc from the LMC's center. Further, the spatial distribution of the outlying GCs is statistically different from the full GC population (Figure 2). However, the kinematically outlying GCs do not show any clustering in their age distribution.
4. *Inclusion of kinematically outlying GCs can bias LMC's mass inference by upto 30%:* We assess the reliability of LMC's enclosed mass estimates derived from GCs as dynamical tracers. Including the outlying GCs can affect the tracer mass estimate by 15-30%, depending on the sub-sample of outliers used (Figure 5). Caution must be exercised while attempting to precisely determine the LMC's DM content using the GC kinematics.

Majority of the GCs that have a high PM difference with the surroundings have also been flagged as outlying in previous investigations of structure (NGC 1978), chemical abundances (NGC 2005) and stellar populations (NGC 2210, Hodge 11) of the LMC GC population

as a whole. These GCs are promising candidates for having an external origin and subsequently being accreted by the LMC.

Further spectroscopic follow up of the outlying LMC GCs is necessary for understanding their individual properties as well as population level properties in detail, as it will give key insights into the assembly history and DM profile of the MW's most prominent satellite galaxy.

ACKNOWLEDGEMENTS

We thank Eugene Vasiliev for sharing with us the code for finding mean and dispersion of proper motions in LMC fields from Vasiliev (2018, 2019a,b). We also thank Paul McMillan for sharing the map of *Gaia* DR3 systematic errors across the same region (Gaia Collaboration et al. 2018). We thank Gurtina Besla, Yumi Choi, Paul Bennet, Laura Watkins, Annapurni Subramaniam, S.R. Dhanush and Himanshu Verma for insightful discussions. Himanshu Rathore would like to acknowledge support from a NASA FINESST fellowship (80NSSC24K1469, PI – G. Besla). The work of Knut Olsen is supported by NOIRLab, which is managed by the Association of Universities for Research in Astronomy (AURA) under a cooperative agreement with the U.S. National Science Foundation. We thank NOIRLab for covering processing costs for the article. This work has used data from the European Space Agency (ESA) mission *Gaia* (<https://sci.esa.int/web/gaia>), processed by the Gaia Data Processing and Analysis Consortium (DPAC, <https://www.cosmos.esa.int/web/gaia/dpac/consortium>). Funding for the DPAC has been provided by national institutions, in particular the institutions participating in the Gaia Multilateral Agreement.

Software: This work made use of Python, and its packages like numpy (van der Walt et al. 2011; Harris et al. 2020), scipy (Virtanen et al. 2020), astropy (Astropy Collaboration et al. 2013, 2018, 2022) and matplotlib (Hunter 2007).

DATA AVAILABILITY

This work used public data available via `astroquery.Gaia`, the Python API to access *Gaia* DR3 data as well as data from Bennet et al. (2022) and the kinematic model of Choi et al. (2022). Processing of spacecraft data is carried out by DPAC.

REFERENCES

- Ahumada, A. V., Vega-Neme, L. R., Clariá, J. J., & Minniti, J. H. 2019, *PASP*, 131, 024101, doi: 10.1088/1538-3873/aae660
- Arora, A., Garavito-Camargo, N., Sanderson, R. E., et al. 2025, *ApJ*, 988, 190, doi: 10.3847/1538-4357/ade30d

- Astropy Collaboration, Robitaille, T. P., Tollerud, E. J., et al. 2013, *A&A*, 558, A33, doi: [10.1051/0004-6361/201322068](https://doi.org/10.1051/0004-6361/201322068)
- Astropy Collaboration, Price-Whelan, A. M., Sipőcz, B. M., et al. 2018, *AJ*, 156, 123, doi: [10.3847/1538-3881/aabc4f](https://doi.org/10.3847/1538-3881/aabc4f)
- Astropy Collaboration, Price-Whelan, A. M., Lim, P. L., et al. 2022, *ApJ*, 935, 167, doi: [10.3847/1538-4357/ac7c74](https://doi.org/10.3847/1538-4357/ac7c74)
- Baird, S. R., & Flower, P. J. 1986, *AJ*, 91, 1336, doi: [10.1086/114108](https://doi.org/10.1086/114108)
- Battaglia, G., Helmi, A., Morrison, H., et al. 2005, *MNRAS*, 364, 433, doi: [10.1111/j.1365-2966.2005.09367.x](https://doi.org/10.1111/j.1365-2966.2005.09367.x)
- Bekki, K., Couch, W. J., Beasley, M. A., et al. 2004, *ApJL*, 610, L93, doi: [10.1086/423372](https://doi.org/10.1086/423372)
- Belokurov, V., & Kravtsov, A. 2024, *MNRAS*, 528, 3198, doi: [10.1093/mnras/stad3920](https://doi.org/10.1093/mnras/stad3920)
- Bennet, P., Alfaro-Cuello, M., del Pino, A., et al. 2022, *The Astrophysical Journal*, 935, 149, doi: [10.3847/1538-4357/ac81c9](https://doi.org/10.3847/1538-4357/ac81c9)
- Besla, G., Kallivayalil, N., Hernquist, L., et al. 2007, *The Astrophysical Journal*, 668, 949, doi: [10.1086/521385](https://doi.org/10.1086/521385)
- Besla, G., Kallivayalil, N., Hernquist, L., et al. 2012, *MNRAS*, 421, 2109, doi: [10.1111/j.1365-2966.2012.20466.x](https://doi.org/10.1111/j.1365-2966.2012.20466.x)
- Besla, G., Martínez-Delgado, D., van der Marel, R. P., et al. 2016, *ApJ*, 825, 20, doi: [10.3847/0004-637X/825/1/20](https://doi.org/10.3847/0004-637X/825/1/20)
- Besla, G., Peter, A. H. G., & Garavito-Camargo, N. 2019, *JCAP*, 2019, 013, doi: [10.1088/1475-7516/2019/11/013](https://doi.org/10.1088/1475-7516/2019/11/013)
- Besla, G., Patton, D. R., Stierwalt, S., et al. 2018, *MNRAS*, 480, 3376, doi: [10.1093/mnras/sty2041](https://doi.org/10.1093/mnras/sty2041)
- Binney, J., & Wong, L. K. 2017, *MNRAS*, 467, 2446, doi: [10.1093/mnras/stx234](https://doi.org/10.1093/mnras/stx234)
- Carraro, G., Ng, Y. K., & Portinari, L. 1998, *MNRAS*, 296, 1045, doi: [10.1046/j.1365-8711.1998.01460.x](https://doi.org/10.1046/j.1365-8711.1998.01460.x)
- Castellani, V., Degl'Innocenti, S., Girardi, L., et al. 2000, *A&A*, 354, 150, doi: [10.48550/arXiv.astro-ph/9911432](https://doi.org/10.48550/arXiv.astro-ph/9911432)
- Chamberlain, K., Besla, G., Patel, E., et al. 2024, *ApJ*, 962, 162, doi: [10.3847/1538-4357/ad19d0](https://doi.org/10.3847/1538-4357/ad19d0)
- Choi, Y., Olsen, K. A. G., Besla, G., et al. 2022, *The Astrophysical Journal*, 927, 153, doi: [10.3847/1538-4357/ac4e90](https://doi.org/10.3847/1538-4357/ac4e90)
- Choi, Y., Nidever, D. L., Olsen, K., et al. 2018, *ApJ*, 866, 90, doi: [10.3847/1538-4357/aae083](https://doi.org/10.3847/1538-4357/aae083)
- Conn, B. C., Jerjen, H., Kim, D., & Schirmer, M. 2018, *ApJ*, 852, 68, doi: [10.3847/1538-4357/aa9eda](https://doi.org/10.3847/1538-4357/aa9eda)
- Correa Magnus, L., & Vasiliev, E. 2022, *MNRAS*, 511, 2610, doi: [10.1093/mnras/stab3726](https://doi.org/10.1093/mnras/stab3726)
- Cowley, C. R., & Stencel, R. E. 2024, arXiv e-prints, arXiv:2408.06161, doi: [10.48550/arXiv.2408.06161](https://doi.org/10.48550/arXiv.2408.06161)
- DeBrae, A., Behroozi, P., & Garavito-Camargo, N. 2025, arXiv e-prints, arXiv:2502.17565, doi: [10.48550/arXiv.2502.17565](https://doi.org/10.48550/arXiv.2502.17565)
- del Pino, A., Fardal, M. A., van der Marel, R. P., et al. 2021, *ApJ*, 908, 244, doi: [10.3847/1538-4357/abd5bf](https://doi.org/10.3847/1538-4357/abd5bf)
- del Pino, A., Libralato, M., van der Marel, R. P., et al. 2022, *ApJ*, 933, 76, doi: [10.3847/1538-4357/ac70cf](https://doi.org/10.3847/1538-4357/ac70cf)
- Dhanush, S. R., Subramaniam, A., & Subramaniam, S. 2024, *ApJ*, 968, 103, doi: [10.3847/1538-4357/ad4453](https://doi.org/10.3847/1538-4357/ad4453)
- D'Onghia, E., & Lake, G. 2008, *ApJL*, 686, L61, doi: [10.1086/592995](https://doi.org/10.1086/592995)
- Dooley, G. A., Peter, A. H. G., Carlin, J. L., et al. 2017, *MNRAS*, 472, 1060, doi: [10.1093/mnras/stx2001](https://doi.org/10.1093/mnras/stx2001)
- Erkal, D., & Belokurov, V. A. 2020, *Monthly Notices of the Royal Astronomical Society*, 495, 2554, doi: [10.1093/mnras/staa1238](https://doi.org/10.1093/mnras/staa1238)
- Fasano, G., & Franceschini, A. 1987, *MNRAS*, 225, 155, doi: [10.1093/mnras/225.1.155](https://doi.org/10.1093/mnras/225.1.155)
- Ferraro, F. R., Mucciarelli, A., Carretta, E., & Origlia, L. 2006, *The Astrophysical Journal*, 645, L33, doi: [10.1086/506178](https://doi.org/10.1086/506178)
- Flower, P. J. 1984, in *IAU Symposium, Vol. 108, Structure and Evolution of the Magellanic Clouds*, ed. S. van den Bergh & K. S. D. de Boer, 31, doi: [10.1017/S0074180900039802](https://doi.org/10.1017/S0074180900039802)
- Foote, H. R., Besla, G., Mocz, P., et al. 2023, *ApJ*, 954, 163, doi: [10.3847/1538-4357/ace533](https://doi.org/10.3847/1538-4357/ace533)
- Foote, H. R., Rathore, H., Besla, G., et al. 2026, arXiv e-prints, arXiv:2601.00946, doi: [10.48550/arXiv.2601.00946](https://doi.org/10.48550/arXiv.2601.00946)
- Forbes, D. A., & Bridges, T. 2010, *MNRAS*, 404, 1203–1214, doi: [10.1111/j.1365-2966.2010.16373](https://doi.org/10.1111/j.1365-2966.2010.16373)
- Gaia Collaboration. 2016, *Astronomy & Astrophysics*, 595, A1, doi: [10.1051/0004-6361/201629272](https://doi.org/10.1051/0004-6361/201629272)
- . 2022, *Gaia Data Release 3: Summary of the content and survey properties*, doi: [10.48550/arXiv.2208.00211](https://doi.org/10.48550/arXiv.2208.00211)
- Gaia Collaboration, Helmi, A., van Leeuwen, F., et al. 2018, *Astronomy & Astrophysics*, 616, A12, doi: [10.1051/0004-6361/201832698](https://doi.org/10.1051/0004-6361/201832698)
- Gaia Collaboration, Luri, X., Chemin, L., et al. 2021, *Astronomy & Astrophysics*, 649, A7, doi: [10.1051/0004-6361/202039588](https://doi.org/10.1051/0004-6361/202039588)
- Gilligan, C. K., Chaboyer, B., Cummings, J. D., et al. 2019, *Monthly Notices of the Royal Astronomical Society*, 486, 5581, doi: [10.1093/mnras/stz1174](https://doi.org/10.1093/mnras/stz1174)
- . 2020, *Monthly Notices of the Royal Astronomical Society*, 494, 1946, doi: [10.1093/mnras/staa822](https://doi.org/10.1093/mnras/staa822)
- Girardi, L. 2016, *Annual Review of Astronomy and Astrophysics*, 54, 95, doi: [10.1146/annurev-astro-081915-023354](https://doi.org/10.1146/annurev-astro-081915-023354)

- Glatt, K., Grebel, E. K., & Koch, A. 2010, *Astronomy & Astrophysics*, 517, A50, doi: [10.1051/0004-6361/201014187](https://doi.org/10.1051/0004-6361/201014187)
- Glatt, K., Gallagher, III, J. S., Grebel, E. K., et al. 2008, *AJ*, 135, 1106, doi: [10.1088/0004-6256/135/4/1106](https://doi.org/10.1088/0004-6256/135/4/1106)
- Goodwin, S. P. 1997, *Monthly Notices of the Royal Astronomical Society: Letters*, 286, L39, doi: [10.1093/mnras/286.3.L39](https://doi.org/10.1093/mnras/286.3.L39)
- Graham, J. A., & Ruiz, M. T. 1974, *Astronomical Journal*, 79, 363
- Harris, C. R., Millman, K. J., van der Walt, S. J., et al. 2020, *Nature*, 585, 357, doi: [10.1038/s41586-020-2649-2](https://doi.org/10.1038/s41586-020-2649-2)
- He, X.-J., Luo, A. L., & Chen, Y.-Q. 2022, *MNRAS*, 512, 1710, doi: [10.1093/mnras/stac484](https://doi.org/10.1093/mnras/stac484)
- Helmi, A. 2008, *The Astronomy and Astrophysics Review*, 15, 145, doi: [10.1007/s00159-008-0009-6](https://doi.org/10.1007/s00159-008-0009-6)
- Helmi, A., Babusiaux, C., Koppelman, H. H., et al. 2018, *Nature*, 563, 85, doi: [10.1038/s41586-018-0625-x](https://doi.org/10.1038/s41586-018-0625-x)
- Hernquist, L. 1990, *ApJ*, 356, 359, doi: [10.1086/168845](https://doi.org/10.1086/168845)
- Hunter, J. D. 2007, *Computing in Science & Engineering*, 9, 90, doi: [10.1109/MCSE.2007.55](https://doi.org/10.1109/MCSE.2007.55)
- Jahn, E. D., Sales, L. V., Wetzel, A., et al. 2022, *MNRAS*, 513, 2673, doi: [10.1093/mnras/stac811](https://doi.org/10.1093/mnras/stac811)
- Jethwa, P., Erkal, D., & Belokurov, V. 2016, *MNRAS*, 461, 2212, doi: [10.1093/mnras/stw1343](https://doi.org/10.1093/mnras/stw1343)
- Jiménez-Arranz, Ó., & Roca-Fàbrega, S. 2025, *A&A*, 698, L7, doi: [10.1051/0004-6361/202555019](https://doi.org/10.1051/0004-6361/202555019)
- Jiménez-Arranz, Ó., Roca-Fàbrega, S., Romero-Gómez, M., et al. 2024, *A&A*, 688, A51, doi: [10.1051/0004-6361/202349058](https://doi.org/10.1051/0004-6361/202349058)
- Jiménez-Arranz, Ó., Romero-Gómez, M., Luri, X., et al. 2023, *Astronomy & Astrophysics*, 669, A91, doi: [10.1051/0004-6361/202244601](https://doi.org/10.1051/0004-6361/202244601)
- Johnson, J. A., Bolte, M., Stetson, P. B., Hesser, J. E., & Somerville, R. S. 1999, *ApJ*, 527, 199, doi: [10.1086/308066](https://doi.org/10.1086/308066)
- Johnson, R. A., Beaulieu, S. F., Gilmore, G. F., et al. 2001, *MNRAS*, 324, 367, doi: [10.1046/j.1365-8711.2001.04291.x](https://doi.org/10.1046/j.1365-8711.2001.04291.x)
- Kallivayalil, N., van der Marel, R. P., Besla, G., Anderson, J., & Alcock, C. 2013, *ApJ*, 764, 161, doi: [10.1088/0004-637X/764/2/161](https://doi.org/10.1088/0004-637X/764/2/161)
- Kim, S., Staveley-Smith, L., Dopita, M. A., et al. 2003, *ApJS*, 148, 473, doi: [10.1086/376980](https://doi.org/10.1086/376980)
- Kruijssen, J. M. D., Pfeffer, J. L., Reina-Campos, M., Crain, R. A., & Bastian, N. 2019, *MNRAS*, 486, 3180, doi: [10.1093/mnras/sty1609](https://doi.org/10.1093/mnras/sty1609)
- Kuzma, P. B., Ferguson, A. M. N., & Peñarrubia, J. 2021, *Monthly Notices of the Royal Astronomical Society*, 507, 1127–1137, doi: [10.1093/mnras/stab2280](https://doi.org/10.1093/mnras/stab2280)
- Lindgren, L., Klioner, S. A., Hernández, J., & et al. 2021, *Astronomy & Astrophysics*, 649, A2, doi: [10.1051/0004-6361/202039709](https://doi.org/10.1051/0004-6361/202039709)
- Lyubenova, M., Kuntschner, H., Rejkuba, M., et al. 2012, *A&A*, 543, A75, doi: [10.1051/0004-6361/201218847](https://doi.org/10.1051/0004-6361/201218847)
- Mackey, A. D., & Gilmore, G. F. 2003, *Monthly Notices of the Royal Astronomical Society*, 338, 85, doi: [10.1046/j.1365-8711.2003.06021.x](https://doi.org/10.1046/j.1365-8711.2003.06021.x)
- . 2004, *Monthly Notices of the Royal Astronomical Society*, 355, 504, doi: [10.1111/j.1365-2966.2004.08343.x](https://doi.org/10.1111/j.1365-2966.2004.08343.x)
- Makarov, D., Khoperskov, S., Makarov, D., et al. 2023, *Monthly Notices of the Royal Astronomical Society*, 521, 3540, doi: [10.1093/mnras/stad757](https://doi.org/10.1093/mnras/stad757)
- Marino, A. F., Przybilla, N., Milone, A. P., et al. 2018, *AJ*, 156, 116, doi: [10.3847/1538-3881/aad3cd](https://doi.org/10.3847/1538-3881/aad3cd)
- Martínez-García, A. M., del Pino, A., Aparicio, A., van der Marel, R. P., & Watkins, L. L. 2021, *MNRAS*, 505, 5884, doi: [10.1093/mnras/stab1568](https://doi.org/10.1093/mnras/stab1568)
- Massari, D., Koppelman, H. H., & Helmi, A. 2019, *Astronomy & Astrophysics*, 630, L4, doi: [10.1051/0004-6361/201936135](https://doi.org/10.1051/0004-6361/201936135)
- McConnachie, A. W. 2012, *AJ*, 144, 4, doi: [10.1088/0004-6256/144/1/4](https://doi.org/10.1088/0004-6256/144/1/4)
- McLaughlin, D. E., & van der Marel, R. P. 2005, *The Astrophysical Journal Supplement Series*, 161, 304, doi: [10.1086/497429](https://doi.org/10.1086/497429)
- Milone, A. P., Cordonì, G., Marino, A. F., et al. 2023, *A&A*, 672, A161, doi: [10.1051/0004-6361/202244798](https://doi.org/10.1051/0004-6361/202244798)
- Miyamoto, M., & Nagai, R. 1975, *PASJ*, 27, 533
- Mucciarelli, A., Ferraro, F. R., Origlia, L., & Pecci, F. F. 2007, *The Astronomical Journal*, 133, 2053, doi: [10.1086/513076](https://doi.org/10.1086/513076)
- Mucciarelli, A., Massari, D., Minelli, A., et al. 2021, *Nature Astronomy*, 5, 1247, doi: [10.1038/s41550-021-01493-y](https://doi.org/10.1038/s41550-021-01493-y)
- Myeong, G., Evans, N., Belokurov, V., Sanders, J., & Koposov, S. 2018, *ApJL*, 863, 28, doi: [10.3847/2041-8213/aad7f7](https://doi.org/10.3847/2041-8213/aad7f7)
- Narloch, W., Pietrzyński, G., Gieren, W., et al. 2022, *Astronomy & Astrophysics*, 666, A80, doi: [10.1051/0004-6361/202243378](https://doi.org/10.1051/0004-6361/202243378)
- Olsen, K. A. G., Hodge, P. W., Mateo, M., et al. 1998, *MNRAS*, 300, 665, doi: [10.1046/j.1365-8711.1998.01860.x](https://doi.org/10.1046/j.1365-8711.1998.01860.x)
- Olsen, K. A. G., & Massey, P. 2007, *ApJL*, 656, L61, doi: [10.1086/512484](https://doi.org/10.1086/512484)
- Olsen, K. A. G., Zaritsky, D., Blum, R. D., Boyer, M. L., & Gordon, K. D. 2011, *ApJ*, 737, 29, doi: [10.1088/0004-637X/737/1/29](https://doi.org/10.1088/0004-637X/737/1/29)
- Olszewski, E. W., Schommer, R. A., Suntzeff, N. B., & Harris, H. C. 1991, *AJ*, 101, 515, doi: [10.1086/115701](https://doi.org/10.1086/115701)

- Olszewski, E. W., Suntzeff, N. B., & Mateo, M. 1996, *Annual Review of Astronomy and Astrophysics*, 34, 511, doi: [10.1146/annurev.astro.34.1.511](https://doi.org/10.1146/annurev.astro.34.1.511)
- Pace, A. B., Erkal, D., & Li, T. S. 2022, *The Astrophysical Journal*, 940, 136, doi: [10.3847/1538-4357/ac997b](https://doi.org/10.3847/1538-4357/ac997b)
- Pagnini, G., Matteo, P. D., Khoperskov, S., et al. 2023, *Astronomy & Astrophysics*, 673, A86, doi: [10.1051/0004-6361/202245128](https://doi.org/10.1051/0004-6361/202245128)
- Patel, E., Kallivayalil, N., Garavito-Camargo, N., et al. 2020, *The Astrophysical Journal*, 893, 121, doi: [10.3847/1538-4357/ab7b75](https://doi.org/10.3847/1538-4357/ab7b75)
- Peacock, J. A. 1983, *MNRAS*, 202, 615, doi: [10.1093/mnras/202.3.615](https://doi.org/10.1093/mnras/202.3.615)
- Perina, S., Cohen, J. G., Barmby, P., et al. 2010, *A&A*, 511, A23, doi: [10.1051/0004-6361/200913459](https://doi.org/10.1051/0004-6361/200913459)
- Pfeffer, J., Lardo, C., Bastian, N., Saracino, S., & Kamann, S. 2021, *MNRAS*, 500, 2514, doi: [10.1093/mnras/staa3407](https://doi.org/10.1093/mnras/staa3407)
- Piatti, A. E. 2014, *ISRN Astronomy and Astrophysics*, 2014, 398182, doi: [10.1155/2014/398182](https://doi.org/10.1155/2014/398182)
- Piatti, A. E. 2022, *Monthly Notices of the Royal Astronomical Society: Letters*, 511, L72, doi: [10.1093/mnrasl/slac010](https://doi.org/10.1093/mnrasl/slac010)
- Piatti, A. E., Keller, S. C., Mackey, A. D., & Costa, G. S. D. 2014, *Monthly Notices of the Royal Astronomical Society*, 444, 1425, doi: [10.1093/mnras/stu1535](https://doi.org/10.1093/mnras/stu1535)
- Piatti, A. E., & Mackey, A. D. 2018, *Monthly Notices of the Royal Astronomical Society*, 478, 2164, doi: [10.1093/mnras/sty1048](https://doi.org/10.1093/mnras/sty1048)
- Pietrzyński, G., Graczyk, D., Gieren, W., et al. 2013, *Nature*, 495, 76, doi: [10.1038/nature11878](https://doi.org/10.1038/nature11878)
- Posti, L., & Helmi, A. 2019, *A&A*, 621, A56, doi: [10.1051/0004-6361/201833355](https://doi.org/10.1051/0004-6361/201833355)
- Rathore, H., Besla, G., Daniel, K. J., & Beraldo e Silva, L. 2025a, *ApJ*, 988, 79, doi: [10.3847/1538-4357/ade0ae](https://doi.org/10.3847/1538-4357/ade0ae)
- Rathore, H., Besla, G., van der Marel, R. P., & Kallivayalil, N. 2025b, *arXiv e-prints*, arXiv:2512.06075, doi: [10.48550/arXiv.2512.06075](https://doi.org/10.48550/arXiv.2512.06075)
- Rathore, H., Choi, Y., Olsen, K. A. G., & Besla, G. 2025c, *ApJ*, 978, 55, doi: [10.3847/1538-4357/ad93ae](https://doi.org/10.3847/1538-4357/ad93ae)
- Reynoso-Cordova, J., Bozorgnia, N., & Piro, M.-C. 2024, *JCAP*, 2024, 037, doi: [10.1088/1475-7516/2024/12/037](https://doi.org/10.1088/1475-7516/2024/12/037)
- Sagar, R., & Pandey, A. K. 1989, *A&AS*, 79, 407
- Sales, L. V., Navarro, J. F., Cooper, A. P., et al. 2011, *MNRAS*, 418, 648, doi: [10.1111/j.1365-2966.2011.19514.x](https://doi.org/10.1111/j.1365-2966.2011.19514.x)
- Sarajedini, A. 2024, *Monthly Notices of the Royal Astronomical Society*, 529, 3998, doi: [10.1093/mnras/stae752](https://doi.org/10.1093/mnras/stae752)
- Sarajedini, A., Grocholski, A. J., Levine, J., & Lada, E. 2002, *AJ*, 124, 2625, doi: [10.1086/343776](https://doi.org/10.1086/343776)
- Schommer, R. A., Suntzeff, N. B., Olszewski, E. W., & Harris, H. C. 1992, *AJ*, 103, 447, doi: [10.1086/116074](https://doi.org/10.1086/116074)
- Sharma, S., Borissova, J., Kurtev, R., Ivanov, V. D., & Geisler, D. 2010, *AJ*, 139, 878, doi: [10.1088/0004-6256/139/3/878](https://doi.org/10.1088/0004-6256/139/3/878)
- Subramaniam, A., & Subramanian, S. 2009, *ApJL*, 703, L37, doi: [10.1088/0004-637X/703/1/L37](https://doi.org/10.1088/0004-637X/703/1/L37)
- van den Bergh, S. 2008, *Monthly Notices of the Royal Astronomical Society: Letters*, 385, L20, doi: [10.1111/j.1745-3933.2008.00424.x](https://doi.org/10.1111/j.1745-3933.2008.00424.x)
- van der Marel, R. P., Alves, D. R., Hardy, E., & Suntzeff, N. B. 2002, *The Astronomical Journal*, 124, 2639–2663, doi: [10.1086/343775](https://doi.org/10.1086/343775)
- van der Marel, R. P., & Cioni, M.-R. L. 2001, *AJ*, 122, 1807, doi: [10.1086/323099](https://doi.org/10.1086/323099)
- van der Walt, S., Colbert, S. C., & Varoquaux, G. 2011, *Computing in Science & Engineering*, 13, 22, doi: [10.1109/MCSE.2011.37](https://doi.org/10.1109/MCSE.2011.37)
- Vasiliev, E. 2018, *MNRAS*, 481, L100, doi: [10.1093/mnrasl/sly168](https://doi.org/10.1093/mnrasl/sly168)
- Vasiliev, E. 2019a, *Monthly Notices of the Royal Astronomical Society*, 484, 2832, doi: [10.1093/mnras/stz171](https://doi.org/10.1093/mnras/stz171)
- . 2019b, *MNRAS*, 489, 623, doi: [10.1093/mnras/stz2100](https://doi.org/10.1093/mnras/stz2100)
- Virtanen, P., Gommers, R., Oliphant, T. E., et al. 2020, *Nature Methods*, 17, 261, doi: [10.1038/s41592-019-0686-2](https://doi.org/10.1038/s41592-019-0686-2)
- Wagner-Kaiser, R., Mackey, D., Sarajedini, A., et al. 2017, *Monthly Notices of the Royal Astronomical Society*, 471, 3347, doi: [10.1093/mnras/stx1702](https://doi.org/10.1093/mnras/stx1702)
- Watkins, L. L., van der Marel, R. P., & Bennet, P. 2024, *ApJ*, 963, 84, doi: [10.3847/1538-4357/ad1f58](https://doi.org/10.3847/1538-4357/ad1f58)
- Werchan, F., & Zaritsky, D. 2011, *The Astronomical Journal*, 142, 48, doi: [10.1088/0004-6256/142/2/48](https://doi.org/10.1088/0004-6256/142/2/48)
- West, M. J., Côté, P., Marzke, R. O., & Jordán, A. 2004, *Nature*, 427, 31, doi: [10.1038/nature02179](https://doi.org/10.1038/nature02179)
- Zivick, P., Kallivayalil, N., Besla, G., et al. 2019, *ApJ*, 874, 78, doi: [10.3847/1538-4357/ab0554](https://doi.org/10.3847/1538-4357/ab0554)

APPENDIX: AGES OF LMC GLOBULAR CLUSTERS

Name of GC	Age [Gyr]	Reference
NGC 1644	1.80	Milone, A. P. et al. (2023)
NGC 1651	2.20	Milone, A. P. et al. (2023)
NGC 1652	2.25	Milone, A. P. et al. (2023)
NGC 1756	0.20	Milone, A. P. et al. (2023)
NGC 1783	1.95	Milone, A. P. et al. (2023)
NGC 1786	12.9	Milone, A. P. et al. (2023)
NGC 1806	1.90	Milone, A. P. et al. (2023)
NGC 1818	0.08	Milone, A. P. et al. (2023)
NGC 1831	0.07	Milone, A. P. et al. (2023)
NGC 1866	0.90	Milone, A. P. et al. (2023)
NGC 1868	1.45	Milone, A. P. et al. (2023)
NGC 1928	13.0	Milone, A. P. et al. (2023)
NGC 1939	13.3	Milone, A. P. et al. (2023)
NGC 1978	2.50	Milone, A. P. et al. (2023)
NGC 1987	1.35	Milone, A. P. et al. (2023)
NGC 2108	1.25	Milone, A. P. et al. (2023)
NGC 2159	0.1	Glatt et al. (2010)
NGC 2162	2.0	Lyubenova et al. (2012)
NGC 2173	2.05	Milone, A. P. et al. (2023)
NGC 2190	1	Piatti (2014)
NGC 2209	1.45	Milone, A. P. et al. (2023)
NGC 2210	12.0	Milone, A. P. et al. (2023)
NGC 2231	0.5	Flower (1984)
Hodge 4	1.7	Sarajedini et al. (2002)
Hodge 11	13.4	Milone, A. P. et al. (2023)
NGC 1835	12.0	Graham & Ruiz (1974)
NGC 1898	11.7	Milone, A. P. et al. (2023)
NGC 1916	11.0	Piatti & Mackey (2018)
NGC 2005	13.1	Milone, A. P. et al. (2023)
NGC 2019	11.0	Piatti & Mackey (2018)

Table 3. Ages of LMC GCs studied in this work. We classify GCs as old if their age is ≥ 10 Gyr, intermediate if their age is from 0.5 to 4 Gyr, and young if their age is ≤ 0.2 Gyr.